

Published in final edited form as:

Curr Pharm Des. 2012 ; 18(24): 3539–3566.

A Physico-Biochemical Study on Potential Redox-Cyclers as Antimalarial and Antischistosomal Drugs

Laure Johann, Don Antoine Lanfranchi, Elisabeth Davioud-Charvet, and Mourad Elhabiri*

Laboratoire de Chimie Bioorganique et Médicinale, European School of Chemistry, Polymers and Materials (ECPM), University of Strasbourg and Centre National de la Recherche Scientifique, UMR 7509, 25, rue Becquerel, F-67087 Strasbourg, France

Abstract

The role of redox enzymes in establishing a microenvironment for parasite development is well characterized. Mimicking human glucose-6-phosphate dehydrogenase and glutathione reductase (GR) deficiencies by redox-cycling compounds thus represents a challenge to the design of new preclinical antiparasitic drug candidates. Schistosomes and malarial parasites feed on hemoglobin. Heme, the toxic prosthetic group of the protein, is not digested and represents a challenge to the redox metabolism of the parasites. Here, we report on old and new redox-cycling compounds – whose antiparasitic activities are related to their interference with (met)hemoglobin degradation and heme crystallization. Three key-assays allowed probing and differentiating the mechanisms of drug actions. Inhibition of β -hematin was first compared to the heme binding as a possible mode of action. All tested ligands interact with the heme π - π dimer with K_D similar to those measured for the major antiparasitic drugs. No correlation between a high affinity for heme and the capacity to prevent β -hematin formation was however deduced. Inhibition of β -hematin formation is consequently not the result of a single process but results from redox processes following electron transfers from the drugs to iron(III)-containing targets. The third experiment highlighted that several redox-active compounds (in their reduced forms) are able to efficiently reduce methemoglobin to hemoglobin in a GR/NADPH-coupled assay. A correlation between methemoglobin reduction and inhibition of β -hematin was shown, demonstrating that both processes are closely related. The ability of our redox-cyclers to trigger methemoglobin reduction therefore constitutes a critical step to understand the mechanism of action of our drug candidates.

Keywords

hematin; β -hematin; antimalarial; antischistosomal; naphthoquinone; xanthone; NADPH-dependent disulfide reductase; redox-cycler

Introduction

Malaria and schistosomiasis are two major tropical infectious diseases caused by *Plasmodia* and *Schistosoma* parasites, respectively. These diseases are ranked first and second among the world's parasitic diseases, in terms of extent of endemic areas, number of infected people and economic burden. Despite numerous antimalarial and antischistosomal agents developed throughout the 20th century, the diseases have not yet been eradicated and no vaccine is available.

*Address correspondence to these authors at the Laboratoire de Chimie Bioorganique et Médicinale, European School of Chemistry, University of Strasbourg, ECPM, UMR 7509 CNRS-Uds, 25, rue Becquerel, 67087 Strasbourg, France; Phone: +33-3-688 526 85, elhabiri@unistra.fr.

The severe form of *P. falciparum* malaria is responsible for the death of less than one million people per year, mainly children below 5 years of age. Multidrug-resistance of malarial strains toward broadly used antimalarial drug treatments (e.g. chloroquine, quinine, sulfadoxine-pyrimethamine) has spread all over the world in the last five decades. Schistosomiasis is a group of widespread and devastating tropical diseases caused by the platyhelminth *Schistosoma* which affects more than 200 million people worldwide, especially in Africa. Praziquantel has been the anthelmintic drug of choice against flatworms for more than 20 years; currently more than 100 million people per year are treated with this drug. If resistant worms develop, schistosomiasis treatment will face a crisis because of the absence of alternative effective drugs or of a sufficiently protective vaccine. Thus, concerning these two neglected diseases, there is an urgent need for new ethical drugs to emerge which should be efficient, safe, cheap to synthesize and which display mechanism(s) of action that counteract the development of resistance.

During the intraerythrocytic cycle of malarial parasites, a large amount of host cell hemoglobin (Table 1) is digested in acidic vesicles and in the final food vacuole. Hemoglobin digestion, as a source of essential nutrients, was also observed to occur in the gut of *Schistosoma* worms [1]. This catabolic process generates indigestible and toxic heme (iron(III) protoporphyrin IX or $\text{Fe}^{\text{III}}\text{PPIX}$, Table 1) with concomitant high fluxes of reactive oxygen species (ROS) inducing oxygen-derived radical reactions and over-oxidation of macromolecules. Both malarial and schistosomal parasites evade the toxicity of the released free heme by expressing two major detoxification pathways, the biocrystallization of heme into a dark brown pigment called hemozoin [2,3] (Hz; the synthetic crystal formed from hemozoin is called β -hemozoin, Table 1) and an efficient thiol network based on the regeneration of thiols catalyzed by NADPH-dependent disulfide reductases [4,5,6] (Figure 1). These flavoenzymes include both glutathione reductases (GR) of *Plasmodium*-infected human erythrocytes identified as targets of antimalarial drugs [7] and the unique multifunctional enzyme, the thioredoxin-glutathione reductase (TGR) [8], specifically found in *Schistosoma*. *Schistosoma mansoni* TGR, which was recently proved to be an essential enzyme for *Schistosoma* worms to maintain the reducing balance, is also a key drug target for antischistosomal drug design [9]. Therefore, throughout the years, the development of antiparasitic agents against blood-feeding parasites like *Plasmodium* parasites and *Schistosoma* worms has been focused on chemical series which target the heme biocrystallization process. Not surprisingly, numerous heme binders sharing common structural motifs – from 4-aminoquinolines [10], quinoline methanols or arylmethanols [11,12], endoperoxides [13], to xanthenes [14,15,16] – kill both malarial and schistosomal parasites.

The malarial parasite indeed prevents damage (oxidative stress) by a cytosolic antioxidant thiol network that is regenerated by NADPH-dependent disulfide oxidoreductases, glutathione reductase (GR; EC 1.8.1.7), thioredoxin reductase (TrxR; EC 1.8.1.9) [4,5], and possibly by lipoamide dehydrogenase (LipDH; EC 1.8.1.4) [17]. Among the most effective ligands of NADPH-dependent disulfide reductases the most potent antiparasitic effects were indeed observed for redox-cyclers acting as subversive substrates of these flavoenzymes (reaction 1 in Scheme 1). Subversive substrates of disulfide reductases are exemplified by methylene blue, 1,4-naphthoquinones, nitrofurans [4,5]. These compounds are reduced *via* 1 or 2 electron(s)-transfer and regenerated in the presence of major oxidants in the parasites (reaction 2 in Scheme 1), as previously shown with the couple metHb(Fe^{III})/oxyHb(Fe^{II}) (Table 1) in the presence of methylene blue or 3-benzoyl menadione derivatives as redox molecules [18,19].

In the majority of reported *in vitro* UV-Vis spectrophotometric studies about hemozoin (hydroxylated or aquo heme or $[(\text{Fe}^{\text{III}}\text{PPIX})(\text{OH})]$ or $[(\text{Fe}^{\text{III}}\text{PPIX})(\text{OH}_2)]$, Table 1)

crystallization, investigations of heme speciation have been carried out in the presence of the potent antimalarial 4-aminoquinolines [20]. This is partly due to the high solubility of these weak bases containing three nitrogen atoms with a broad range of pK_a values. Upon protonation of the quinoline ($pK_a \sim 8$) and of the terminal amino group ($pK_a \sim 11$) of the side chain, the solubility of the compounds is drastically increased in aqueous media, rendering “comfortable” the physicochemical analysis of the heme:drug complexes *in vitro* under varying pH conditions. However, structurally distinct chemical series with limited solubility were reported to display antimalarial activities and inhibition effects on hemozoin formation. Because of the broad range of drug solubility, many *in vitro* assays using heme at different pH values can lead to misinterpretations if precipitation of the drug occurs, especially if the assays are based on heme absorbance at one fixed wavelength [21]. Furthermore, as it has been clearly demonstrated in recent reports [18,19], inhibition of hemozoin formation is not the result of only one process, i.e. of ligand binding to the π - π heme dimer. It can also originate from redox processes following electron transfer reactions from the drug to the iron(III) of two relevant targets heme and methemoglobin (noted metHb or metHb(Fe^{III}), Table 1). In particular, heme(Fe^{II}) is an inhibitor of heme crystallization [22]. To illustrate metHb(Fe^{III}) conversion by redox cyclers, we recently demonstrated the ability of reduced 3-benzoylnaphthoquinones (i.e. dihydronaphthoquinones) to generate oxyHb(Fe^{II}) (Table 1) as a mechanism of antimalarial action of 3-benzoylnaphthoquinone derivatives [18,19].

Plasmodium parasites digest methemoglobin (metHb(Fe^{III})) faster than oxyhemoglobin (oxyHb(Fe^{II})) [23] and hemoglobin oxidation to methemoglobin in the acidic vesicles/food vacuole is the basis of creating space for parasite growth. Consequently, the reduction of metHb(Fe^{III}) to oxyHb(Fe^{II}) by redox-active agents is expected to slow down both metHb(Fe^{III}) digestion and the growth rate of the parasite. Another reason for targeting metHb(Fe^{III}) reduction is that ferric hemoglobin is not able to transport oxygen; metHb(Fe^{III}) elevation in brain blood vessels of infected host, for instance, contributes to hypoxia and cerebral malaria [24]. Thus, the reduction of redox-active agents by NADPH in reactions mediated by disulfide reductases and their oxidation, from their reduced forms, in spontaneous reactions with ferric species of heme and hemoglobin might contribute both to the elevation of free heme level and to interference with hemozoin formation in the parasites. Both events – oxidizing the reductants and reducing the oxidants in a continuous redox cycle (Figure 1) – are expected to contribute to the elimination of the parasites [18,19]. This strategy is well illustrated by recent findings about the mode of action of the antimalarial drug methylene blue [25] and a novel series of 3-benzylmenadione derivatives involved in a cascade of redox reactions in the parasites as part of the putative mode of action [18,19].

In this paper, it is our goal to describe three key-assays that can be used as probes to differentiate between distinct mechanisms of antimalarial (Figure 1) or antischistosomal drug actions and that can be employed to identify hemozoin inhibitors both *in vitro* and *in vivo*. Quasi-physiological conditions applied to these assays would bring high benefit to rationalize the effects of well-controllable inhibitors. Several different assays based on the speciation of heme in aqueous solutions with varying pH have been developed for studying the interaction capabilities of the drugs with metHb(Fe^{III}) at pH 6.9 or heme at pH ~5 and pH 7.4. Two low solubility-featured compound series, antimalarial 1,4-naphthoquinones and antischistosomal xanthenes, were selected in this present report to illustrate the most frequently applied spectrophotometric assays.

Thermodynamics and Structural Aspects of Ferriprotoporphyrim

From Heme to Hemozoin in Blood-Feeding Plasmodium and Schistosoma Parasites

As part of its complex life cycle, the parasite invades, grows and multiplies within the host's red blood cells. The parasite digests a high quantity of hemoglobin from the host cell cytoplasm (Figure 1) using a cytostome and transports the hemoglobin to its acidic digestive vacuole (pH 5.0–5.5) [26]. In the process of hemoglobin digestion, free heme (ferriprotoporphyrim, noted **Fe^{III}PPIX**, Figure 2) is produced, which is highly toxic for the parasite.

Indeed, heme is an ubiquitous and essential molecule playing key roles in biological processes like oxygen transport, respiration, photosynthesis and drug detoxification. However, due to its intrinsic properties, heme can cause numerous deleterious effects within the cell [27]. Due to its amphiphilic features, heme binds to phospholipid membranes altering their permeability and selectivity, and ultimately leading to cell lysis [28]. Because of its pro-oxidant character, heme is also capable of generating free reactive radicals through the decomposition of organic peroxides. These reactive oxygen species (ROS) mediate lipids peroxidation resulting in protein cross-linking and nucleic acid modifications. To overcome this free **Fe^{III}PPIX**-induced toxicity, efficient biomineralization of heme into a highly insoluble and relatively “unreactive” crystal called hemozoin (Hz or malaria pigment) is essential for its detoxification. The overlapping of the iron(III) porphyrins decrease the active surface and consequently significantly decreases the pro-oxidant capacity [29]. Nevertheless, far from being an “inert” pigment, hemozoin has also a redox activity, consistent with previous studies showing that hemozoin could induce lipid peroxidation in human monocytes [30,31]. Hemozoin is nowadays widely considered as the main key target of many antimalarial agents, in particular 4-aminoquinolines. Indeed, 4-aminoquinoline antimalarials such as chloroquine (Table 2) have been demonstrated to inhibit hemozoin formation by binding either to free **Fe^{III}PPIX** preventing biomineralization reactions [32].

Fe^{III}PPIX Speciation in Aqueous Solution and Relevance to Hemozoin Formation

The deeper understanding of the ferriprotoporphyrim (heme) speciation in solution is therefore of essential interest to unravel its role in biomineralization processes (formation of the hemozoin crystal) in malarial parasites and *Schistosoma* worms. The evaluation of the nature, the stoichiometry and the strength of ferriprotoporphyrim **Fe^{III}PPIX** complexes with antimalarial and antischistosomal redox biosensors, a focus of our ongoing research work and of this present report, is of fundamental importance. The nature of the hematin dimer in solution (μ -oxo [33] / π - π [34] / μ -Pr [35]), which has been established to be an important building block during the formation of hemozoin, was (and is still) a subject of interest and debates for more than sixty years. Iron(III) metalloporphyrins can undergo various equilibria in solution (self-association or dimerization, oligomerization) and protolytic reactions depending on the physico-chemical conditions of the medium (solvent, pH, ionic strength, temperature...). In 1947, J. Shack and W. M. Clarke [36] were among the first scientists to demonstrate that **Fe^{III}PPIX** displays intricate speciation behavior in aqueous solution. More than twenty years later, S. B. Brown et al. [37] showed, thanks to absorption spectrophotometry, that **Fe^{III}PPIX** can undergo dimerization in aqueous solution and first proposed this dimer to be a μ -oxo species (Figure 3) [38].

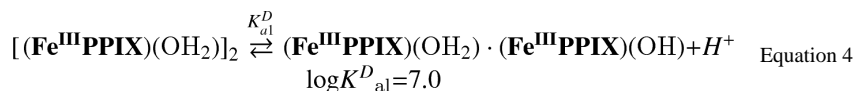
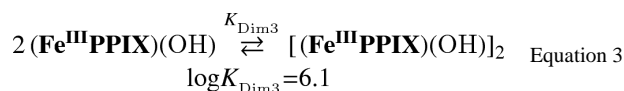
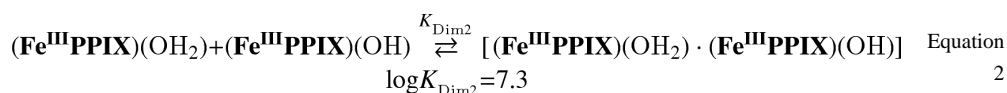
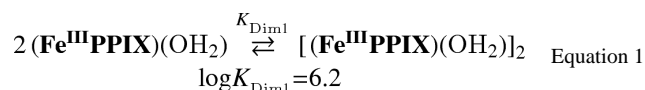
Since then, heme behavior in aqueous solutions was a matter of several contradictory reports on the nature and the speciation properties of the **Fe^{III}PPIX** dimer. T. J. Egan and his coworkers [20] recently established that **Fe^{III}PPIX**(H₂O/HO⁻) does not spontaneously form a μ -oxo dimer in aqueous mixtures of protic solvent, but rather a cofacial π - π dimer (Figure 3B). The μ -oxo dimer (Figure 3A) is rather a predominant species in aqueous mixtures of

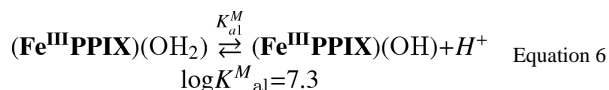
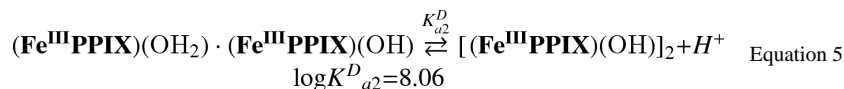
aprotic solvents or in detergent solutions (e.g. with 10% pyridine in an aqueous solution of $\text{Fe}^{\text{III}}\text{PPIX}$ at 0.1 M NaOH or in aqueous mixtures containing aprotic solvent such as 5.64 M DMSO, acetone or DMF at pH 10). The influence of experimental conditions (nature of the pH, protic or aprotic character of the solvent...) has been clearly demonstrated and reviewed in the report published by T. J. Egan and his coworkers [20]. In addition, this μ -oxo dimer is characterized by an absorption band in the visible region centered at about 575 nm (together with a shoulder at about 600 nm).

The thermodynamics of the $(\text{Fe}^{\text{III}}\text{PPIX})_2$ dimer formation (both under a π - π [39] or μ -oxo [20,40] state) has been recently revisited and thoroughly described. For instance, at pH \sim 7.4, which corresponds to acidity which was considered in our thermodynamic investigations, the $(\text{Fe}^{\text{III}}\text{PPIX})_2$ π - π dimer constitutes the major species in a wide range of $[\text{Fe}^{\text{III}}\text{PPIX}]_{\text{tot}}$ (Figure 4A), while the $(\text{Fe}^{\text{III}}\text{PPIX})_2\text{O}$ μ -oxo dimer is a minor species for $[\text{Fe}^{\text{III}}\text{PPIX}]_{\text{tot}}$ below $10^{-2.5}$ M in aqueous 5.64 M DMSO (40% v/v) solutions (Figure 4B). These physico-chemical considerations support the fact that the $(\text{Fe}^{\text{III}}\text{PPIX})_2$ π - π dimer is by far a more stable bio-edifice under quasi-physiological conditions with respect to the $(\text{Fe}^{\text{III}}\text{PPIX})_2\text{O}$ μ -oxo dimer except if not physiological conditions are used ($[\text{Fe}^{\text{III}}\text{PPIX}]_{\text{tot}} \gg 3.16$ mM, presence of aprotic solvents such as DMSO, high pH values – pH > 10...).

These physico-chemical results pointed out the intricacy of the behavior of Fe(III) protoporphyrin IX in aqueous solution [20,39]. The nature and the arrangement of the species were demonstrated to be closely dependent on numerous physico-chemical parameters such as the medium acidity, the $\text{Fe}^{\text{III}}\text{PPIX}$ concentrations, the temperature, the electrolyte concentration and/or the nature of the solvents (polarity, proticity...). These physico-chemical factors determine whether $\text{Fe}^{\text{III}}\text{PPIX}$ monomers, π - π , μ -oxo (and at lesser extend μ -Pr – Figure 3C) dimers or larger aggregates are formed in solution.

Figure 5 displays the distribution diagrams of the protonated species of the $(\text{Fe}^{\text{III}}\text{PPIX})_2$ π - π dimer as a function of pH. The dimerization constants as well as the protonation constant of $[(\text{Fe}^{\text{III}}\text{PPIX})(\text{OH})]$ monomer and of $[(\text{Fe}^{\text{III}}\text{PPIX})_2(\text{H}_2\text{O})_2]$ π - π dimer [25,39] have been considered (equations 1–6) to calculate these speciation diagrams.





For the $(\text{Fe}^{\text{III}}\text{PPIX})_2$ π - π dimer, the two iron(III) protoporphyrins adopt a face to face cofacial arrangement ($\text{Fe}^{\text{III}}\text{PPIX} \cdots \text{Fe}^{\text{III}}\text{PPIX}$ interplane distance of 4.42(9) Å – see the example of hemin π - π dimer in Figure 3B) [41] and the two ferric cations are pentacoordinated with a water molecule completing the Fe(III) coordination sphere. The bisquo complex $[(\text{Fe}^{\text{III}}\text{PPIX})(\text{OH}_2)]_2$ can undergo two successive deprotonations to afford the mono- or the bis(hydroxo) species (equations 4 and 5). Therefore, the $(\text{Fe}^{\text{III}}\text{PPIX})_2$ π - π dimer exists in aqueous solution under three different protonated states, namely $[(\text{Fe}^{\text{III}}\text{PPIX})(\text{OH}_2)]_2$, $[(\text{Fe}^{\text{III}}\text{PPIX})(\text{OH}_2) \cdot (\text{Fe}^{\text{III}}\text{PPIX})(\text{OH})]$ and $[(\text{Fe}^{\text{III}}\text{PPIX})(\text{OH})]_2$ (the charges have been omitted for the sake of clarity). The distribution diagrams presented in Figure 5 show that the biomineralization processes may be related to the formation below pH 6 of the bisquo π - π species $[(\text{Fe}^{\text{III}}\text{PPIX})(\text{OH}_2)]_2$. The water molecules are more labile than the hydroxyl groups and are hence more easily displaced by the propionate groups of the side arms of an adjoining ferriprophyrinic unit ((i) at pH ~ 6, the propionic acids are deprotonated; (ii) the corresponding pK_a values have been calculated to be ~ 3.5 [42] in anionic (SDS) or neutral (TX-100) surfactants). This feature is expected to be one of the key parameters in biomineralization process of hematin. These speciation and protolytic properties of Fe(III) protoporphyrin IX also demonstrate that there is a narrow pH window (3.5 < pH < 6) suitable for biomineralization (e.g. the pH of the acidic (pH ~ 5.0–5.5) digestive vacuole of *P. falciparum* and of the worms gut [1] is well suited for hemozoin nucleation and growth). Competition in favor of protonation of the propionate units (pH < 3) or deprotonation of the bisquo $[(\text{Fe}^{\text{III}}\text{PPIX})(\text{OH}_2)]_2$ species (pH > 6) prevent hemozoin formation. These speciation curves also indicate that aquo/hydroxo complex is the predominant species at pH 7.4, the acidity which was chosen for the binding studies reported in this work. Lastly, these studies confirmed that $\text{Fe}^{\text{III}}\text{PPIX}$ spontaneously and exclusively dimerizes in solution even under non physiological conditions ($[\text{Fe}^{\text{III}}\text{PPIX}]_{\text{tot}} > 0.4$ mM) but does not form higher aggregates in aqueous solution above pH 5–6.

Hemozoin and β -Hematin X-Ray Structural Data

Hemozoin and models of hemozoin (β -hematin) [35,41] have been extensively analyzed in the past few years, and led recently to new sights about their biomineralization properties. Until very recently, hemozoin [35] and β -hematin were both regarded as repetitive occurrence of μ -Pr dimers (see vide infra for β -hematin) and the π - π stabilizing interactions were considered only in the context of crystal packing [35].

The repeat unit (triclinic unit cell) of β -hematin can be regarded as a centro-symmetric heme cyclic dimer, where the two $\text{Fe}^{\text{III}}\text{PPIX}$ units are linked through iron-carboxylate bonds ($\text{RCOO}^- \cdots \text{Fe}^{\text{III}}\text{PPIX}$ distance of 1.886(2) Å) between the propionate side-chain of one molecule and the central Fe atom of the other (μ -Pr mode, Figure 3C). The dimers are π -stacked in a similar fashion to that typical of molecular crystals of porphyrins (large interplanar distance and small lateral overlap between the porphyrin moieties). Additional stabilization is gained from the dispersion interactions between the methyl and the vinyl side-chains of the adjacent dimers. Lastly, these structural studies also revealed hydrogen-

bonding interactions, involving the remaining propionate side chains (averaged $O\cdots O = 2.8 \text{ \AA}$), which link the dimers into a symmetrical two-dimensional matrix.

The crystal structure data of hemozoin from *Plasmodium falciparum* was solved at a resolution of 2.4 \AA by powder diffraction data [41,43]. In this study, it was proposed that the driving forces for the $\text{Fe}^{\text{III}}\text{PPIX}$ self-association are constituted of two different modes of interactions. The first one involves strong π - π interactions ($\text{Fe}^{\text{III}}\text{PPIX}\cdots\text{Fe}^{\text{III}}\text{PPIX}$ interplane distance of $4.42(9) \text{ \AA}$) which initiate the crystal formation. In addition, the π - π dimers are interacting intermolecularly through iron(III)-carboxylate linkages (μ -Pr interaction - Figure 3C $-\text{RCOO}^-\cdots\text{Fe}^{\text{III}}\text{PPIX}$ distance of $1.91(8) \text{ \AA}$) stabilizing the crystal structure.

Analyses of these two X-ray data revealed that the structures of hemozoin and β -hematin are very similar even though they were analyzed differently (μ -Pr *versus* π - π mode). However, many open issues still remain regarding the mechanisms by which hemozoin nucleates and grows. Hemozoin appears to be chemically and spectroscopically identical to β -hematin which is formed by heating $\text{Fe}^{\text{III}}\text{PPIX}$ in concentrated acid at 60°C [43], or at physiological temperatures if a suitable lipid-water interface is provided [44].

Major Antimalarial Drugs Inhibiting Hemozoin Formation

Several series of antimalarial drugs were reported to exert to different extents their antimalarial activity by enhancing free heme toxicity through the inhibition of hemozoin formation. However, no direct correlation between the antimalarial activity (*in vitro* and *in vivo*) and the inhibition of hemozoin or β -hematin formation was clearly established unless the lipophilicity and the protonation constants ($\text{p}K_a$) of the tested compounds have been taken into account [45]. The $\text{p}K_a$ values are important to consider in the case of antimalarial drugs which mainly interact with the Fe(III) protoporphyrin through drug-Fe(III) fifth axial coordination bond. The binding constants usually follow the order of the $\text{p}K_a$ values that are tuned by substituent-induced electronic effects [46]. Major families of antimalarial drugs inhibiting hemozoin formation involve methylene blue and their derivatives, quinolones, xanthenes, azoles, isonitriles [47, 48].

The first synthetic antimalarial drug, methylene blue (Table 2), a tricyclic phenothiazine blue cationic dye and some of its derivatives, have been shown to interact with heme and their antimalarial activities correlated well with the abilities to inhibit β -hematin formation [49]. It was also known as an effective subversive substrate of various NADPH-dependent disulfide reductases [7b]. We recently reported that methylene blue firmly binds to the hematin π - π dimer forming a (hematin)₂: MB complex (MB = methylene blue) under quasi-physiological conditions (pH 7.4) [25]. This effect is likely to contribute to the inhibition of hemozoin formation in *Plasmodium falciparum* and to the increase of the concentration of parasite-toxic heme. On the other hand, the reduction of metHb(Fe^{III}) to oxyHb(Fe^{II}) by NADPH is efficiently catalyzed by methylene blue and glutathione reductase (metHb reduction rate constant of $991 \pm 44 \text{ M}^{-1} \text{ s}^{-1}$). Thus, the redox properties of methylene blue can also affect the digestion of metHb by the malarial parasites and inhibit *P. falciparum* growth.

The 4-aminoquinolines are certainly the most important and studied class of antimalarial drugs considered until now that act by targeting the parasite specific hemoglobin digestion pathway. For example, chloroquine (Table 2), a famous member of this 4-aminoquinoline family of compounds, accumulates in the acidic digestive vacuole of the parasite [50]. It was shown to interact with the μ -oxo dimer of oxidized heme, thereby preventing hemozoin formation [51]. Chloroquine strongly binds to $\text{Fe}^{\text{III}}\text{PPIX}$ leading to a 1:1 complex with

association constants $\log K_A \sim 5-6$ ($K_D \sim 2-15 \mu\text{M}$) at pH 7.5 [12,51,57,58,59,60]. The π - π interaction between chloroquine and the conjugated π -system of heme is believed to govern and stabilize the formation of adducts. Free heme and heme-chloroquine complexes may kill parasites by inducing severe oxidative stress [52], which successively leads to peroxidation of parasite membrane lipids, damage of DNA, oxidation of protein and ultimately, death of the parasite. Quinine (Table 2), a quinoline methanol antimalarial (another important member of the quinoline family) was also shown to interact with **Fe^{III}PPIX** but less efficiently than chloroquine by forming a 1:1 complex characterized by association constants $\log K_A \sim 4.1-4.3$ ($K_D \sim 50-80 \mu\text{M}$) at pH 7.5 [51]. Quinine was reported to inhibit hemozoin formation [53]. Even though many spectroscopic reports have been published [54], the lack of structural data related to the interactions of 4-aminoquinoline antimalarial drugs with heme-containing targets renders difficult the design and the development of novel compounds. The recent elucidation of the crystal structure of the complex of halofantrine with **Fe^{III}PPIX** by T. J. Egan and his coworkers [12] shed light on the existing interactions with antimalarials, especially the arylmethanols. A three-point interaction coordination complex that involves π - π stacking, O-Fe^{III} coordination and intramolecular hydrogen bonding was shown. In addition to the π -stacking of the phenanthrene ring of halofantrine over the porphyrin ring system, the drug coordinates to the iron(III) centre of **Fe^{III}PPIX** through its alcohol unit. This arylmethanol/**Fe^{III}PPIX** complex is also stabilized through an additional intermolecular hydrogen bond occurring between the protonated terminal nitrogen atom of halofantrine and a propionate side arm of the **Fe^{III}PPIX** monomer. This salt bridge formation is suggested to interrupt the formation of the hemozoin dimer precursor produced during the heme detoxification pathway and satisfactorily accounted for the strong activity of the two active antimalarial drugs quinidine and quinine. By contrast, formation of comparable salt bridges with the inactive 9-epiquinidine and 9-epiquinine epimers induces more constrained species and necessitates much higher energy costs.

Xanthenes have been identified as another potent class of antimalarial compounds [55]. Xanthenes are supposed to act in a unique fashion to kill *Plasmodium* parasites through the formation of soluble complexes with heme, thereby inhibiting the process of hemozoin formation [15]. In particular, xanthenes bearing hydroxyl groups at both the 4- and 5-positions, especially when paired with neighboring 3- and 6-substituted hydroxyls, demonstrated the most potent activity to inhibit hemozoin formation. To unravel the mechanism by which these xanthenes inhibit *Plasmodium* growth, spectroscopic and physico-chemical analyses were performed on the 4,5-dihydroxyxanthone (Table 2). The heme:xanthone complex stoichiometry in aqueous solution was found to be 1:2. This interaction is non-cooperative and exhibited a heme complex dissociation constant K_D of 5.1 μM at pH 5.8. The strength of the heme:xanthone interaction is comparable to those measured for the quinoline-based antimalarial drugs chloroquine and quinine (Table 2) [56]. The heme:xanthone complex formation was found to be both pH and solvent dependent, with strong evidences that the xanthone carbonyl moiety firmly interacts with the iron(III) metallic center of the hematin dimer. Hydrogen bonds between the hydroxyl groups of the xanthone (in positions 4 and 5) and the propionate side chains of heme, as well as π - π stacking between both aromatic π systems appeared to contribute to the overall stability of the xanthone-heme complex. It was concluded that this interaction is responsible for the activity of the 4,5-dihydroxyxanthone against *Plasmodium* through effective inhibition of hemozoin formation.

Synthesis and Physico-Biochemical Studies of Xanthone and 1,4-Naphthoquinone Derivatives targeting Iron(III)-Hemoglobin catabolites

Objectives

We now described a thorough physico-biochemical study of six compounds (Figure 6), which was conducted to gain a deeper understanding of the mechanism of action by which xanthone [16,63] and 1,4-naphthoquinone substrates could act as potential inhibitors of β -hematin crystallization through redox-cycling and exert antimalarial or antischistosomal activities. *Plasmodium* and *Schistosoma* parasites digest methemoglobin, resulting from endogenous oxidation of hemoglobin, as a source of essential nutrients (aminoacids) and detoxify the toxic free heme released during methemoglobin digestion *via* its biocrystallization into an insoluble and “inert” crystal called hemozoin (or malaria pigment or *Schistosoma* pigment, Figure 1). Considering that the process of hemoglobin (or methemoglobin) digestion is common to both *Plasmodium* and *Schistosoma* parasites, it was first of interest to study the ability of our compounds to interact with heme in solution, which is usually anticipated to be a first prerequisite when targeting hemozoin formation.

The ability to inhibit β -hematin crystallization was then evaluated and compared with the heme binding properties of our substrates as it is generally accepted as a plausible mode of action of the known antimalarial and antischistosomal drugs (*vide supra*, Table 2). Here, we investigated the ability of redox-active compounds – the naphthoquinones and xanthenes – to inhibit β -hematin formation, not only on the sole basis of hematin binding but also on the basis of electron transfer reactions. Hence, we evaluated if, under their reduced states – the compounds could trigger metHb(Fe^{III}) reduction into oxyHb(Fe^{II}) as a critical step for potential antiparasitic mechanism of actions.

Synthesis of Xanthenes via Palladium-Catalyzed C-H Addition to Nitriles

The synthesis of four xanthenes **1** to **4**, and of two 1,4-naphthoquinone derivatives **5** and **6** was performed to provide key-compounds useful for the physico-biochemical studies.

A rapid and easy two-step synthetic route to xanthenes with excellent yields involving palladium-catalyzed CH-addition to nitriles followed by aromatic nucleophilic substitution S_NAr was followed to synthesize the xanthenes (Scheme 2) [64].

The two-steps Larock's strategy to obtain simple xanthenes was used in order to prepare useful compounds for further structure-activity relationship studies. The 2-methoxy-9H-xanthen-9-one (xanthone **3**) was synthesized in three steps (Scheme 3). Commercially available 1,4-dimethoxybenzene (2 equiv.), 2-fluorobenzonitrile (1 equiv.), Pd(OAc)₂ (0.1 equiv.), DMSO and TFA were used as starting materials and heated at 95 °C for 24 h. The (2,5-dimethoxyphenyl)(2-fluorophenyl)methanone **3a** was obtained as colorless oil with 85% yield after flash chromatography. Compound **3a** was then selectively demethylated by dropwise addition of BBr₃ (1 equiv.) at 0 °C in DCM for 1 h to give the (2-fluorophenyl)(2-hydroxy-5-methoxyphenyl)methanone **3b** with 86% yield. The 2-methoxy-9H-xanthen-9-one **3** was finally obtained with 61% yield after a S_NAr type reaction in the presence of 2.0 equivalents of potassium carbonate. The synthesis of both benz[*c*]xanthen-7-ones (shorten as benzoxanthenes) **1** and **2** started from the corresponding naphthol instead of the phenol and the naphthol intermediate was submitted to the aromatic nucleophilic substitution under basic conditions (K₂CO₃). Both benzoxanthenes **1** and **2** were produced with 69 and 86 % yield, respectively.

To evaluate the influence of fluorinated substituents in the xanthone skeleton on the biological activity, a fluorine xanthone derivative was synthesized. Commercially available

4-methoxy-3,5-difluorophenol (2 equiv.), 2-fluorobenzonitrile (1 equiv.), Pd(OAc)₂ (0.1 equiv.), DMSO and TFA were used as starting materials and heated at 95 °C for 24 h (Scheme 4). The (2,4-difluoro-6-hydroxy-3-methoxyphenyl)(2-fluorophenyl)methanone **4a** was obtained with 14% yield after flash chromatography. This result suggested that the introduction of fluorine atoms in the phenol reagent dramatically decreased the yield of the reaction. Compound **4a** underwent S_NAr type reaction in the presence of 2.0 equivalents of potassium carbonate to obtain 2,4-difluoro-3-methoxy-9H-xanthen-9-one **4** with 53% yield.

UV-visible Absorption Spectrophotometric Titration of Hematin

Principle of the Assay

The affinity of our compounds for hematin was investigated by UV-visible absorption spectrophotometry at pH 7.5, a pH which prevents hematin crystallization (Figure 5). It is noteworthy that under these pH conditions, **Fe^{III}PPIX** predominantly exists as a π - π dimer with one Fe(III) center being coordinated by a water solvent (fifth axial ligand) molecule and the second one with a hydroxyl ligand ($[(\text{Fe}^{\text{III}}\text{PPIX})(\text{OH}_2)].(\text{Fe}^{\text{III}}\text{PPIX})(\text{OH})$] species).

An absorption ($300 \text{ nm} < \lambda < 800 \text{ nm}$) spectrophotometric titration of an aqueous hematin solution ($\sim 3 \times 10^{-5} \text{ M}$ in 0.2 M sodium hepes buffer) at pH 7.5 was carried out by adding microvolumes of a stock solution of the substrate ($\sim 5\text{--}9 \times 10^{-4} \text{ M}$ in DMSO). Aliquots of 5 to 20 μL of the stock substrate solution were added to the reaction mixture and the UV-visible absorption spectra were recorded after each addition. Special care was taken to ensure that equilibrium was attained after each addition.

Spectrophotometric Properties of Hematin

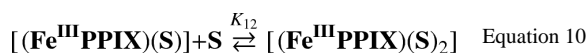
The high-spin **Fe^{III}PPIX** possesses a spin of $S = 5/2$ with all half-filled d-orbitals in close proximity with the porphyrin HOMO and LUMO. This results in a strong overlap between the porphyrin π - π^* ($e_g \pi^*$ excited state orbitals) and the **Fe^{III}** d transitions (d_{yz}, d_{xz} orbitals). This is consequently reflected by broad Q bands in the visible absorption region. Similarly to ferric high spin derivatives of myoglobin and hemoglobin, the formation of a characteristic charge transfer band CT (also called band III ($a_{2u} \rightarrow d_{yz}$) [65,66]) centered at $\sim 613 \text{ nm}$ (Figure 7) can be observed. These spectroscopic characteristics are markedly different from those of the μ -oxo **Fe^{III}PPIX** dimer (absorption in the visible at $\sim 575 \text{ nm}$ together with a shoulder at $\sim 600 \text{ nm}$) thus allowing to precisely probe their occurrence in solution. In addition, exciton transfer occurs from electronic interaction by direct overlap of the π orbitals of the porphyrins (face to face cofacial arrangement for the two **Fe^{III}PPIX** subunits within the π - π dimer) and electron exchange between the individual chromophores. This excitonic coupling in the ground state breaks the degeneracy of the B (or Soret absorption band) excited state, giving rise to two Soret bands lying at 383 nm and 364 nm (Figure 7). This broad and split Soret band is therefore an apparent spectroscopic signature of the presence of the **Fe^{III}PPIX** π - π dimer in solution ($K_{\text{Dim}} = 10^{6.8} \text{ M}^{-1}$ at pH ~ 7.5 , Equations 1–5).

Upon addition of the substrate, concomitant bathochromic shifts and narrowing of the Soret band were observed for all the substrates emphasizing the formation of complexes with hematin π - π dimer. The association constants K_A (M^{-1}), the dissociation constants (μM) and the stoichiometries of the species at equilibrium have been determined by processing the spectrophotometric data with the Specfit program [67,68,69,70,71,72]. Specfit adjusts the stability constants and the corresponding molar extinction coefficients ($\text{M}^{-1} \text{ cm}^{-1}$) of the species at equilibrium.

Spectrophotometric Titrations of the Hematin π - π Dimer by the Substrates at pH 7.5

Xanthenes and Benzoxanthenes—The series of the four xanthenes (compounds **1** to **4**, Figure 6) was studied to evaluate their ability to interact with hematin π - π dimer in 0.2 M sodium hepes buffer pH 7.5 and at $T = 25$ °C. The spectrophotometric titrations of the benzoxanthone **2** (Figure 8) and of xanthone **4** (Figure 9) are given as representative examples.

Benzoxanthone **2** is structurally similar to **1**, the only difference being the substitution by a trifluoromethyl group in **2**. In addition, benzoxanthenes **1** and **2** both possess a hydroxyl unit in position 2 which is methylated. Although this 2-hydroxyl site is not capable to coordinate the Fe(III) center of hematin, our absorption spectrophotometric titrations (Figure 8A), however, revealed the formation of complexes. Upon addition of the substrates **1** or **2**, a narrowing of the broad and split Soret band, characteristic of the hematin π - π dimer, is observed. In addition, a concomitant bathochromic shift of the Soret band is observed and the intensity of the CT absorption of the hematin π - π dimer is decreasing. These data strongly suggest a loss of the excitonic coupling which characterizes the $(\text{Fe}^{\text{III}}\text{PPIX})_2$ π - π dimer (vide supra) and the formation a π - π complexes (or Charge Transfer CT) complexes with benzoxanthenes **1** and **2**. For benzoxanthone **1**, the statistical processing of the absorption data revealed the formation of a $[(\text{Fe}^{\text{III}}\text{PPIX})(\mathbf{1})]$ complex characterized by an association constant of $\log K_{11} = 5.9 \pm 0.01$ (Equation 11, $K_D = 1.26$ μM). The formation of this 1:1 species is in agreement with the dissociation of the hematin π - π dimer and the subsequent alteration of the broad and split Soret band to a sharp and intense absorption being bathochromically shifted. By contrast, two species, namely $[(\text{Fe}^{\text{III}}\text{PPIX})_2(\mathbf{2})]$ ($\log \beta_{21} = 12.5 \pm 0.1$, Equation 7) and $[(\text{Fe}^{\text{III}}\text{PPIX})(\mathbf{2})_2]$ ($\log \beta_{12} = 10.2 \pm 0.2$, Equation 9) were characterized with benzoxanthone **2** which bears an additional trifluoromethyl group. Taking into account the apparent dimerization constant of $\text{Fe}^{\text{III}}\text{PPIX}$ measured at pH 7.5 ($\log K_{\text{Dim}} = 6.82$, Equations 1–5, 12), we can accordingly calculate the successive association constant ($\log K_{21} = 5.7 \pm 0.1$, Equation 8) as well the corresponding dissociation constant ($K_D = 2$ μM).



A possible explanation for this striking dissimilar binding behavior observed for benzoxanthenes **1** and **2** is that, because of steric hindrance and electronic constrains (i.e. electron-withdrawing effects) induced by the CF_3 group and its position of substitution, a

single binder **2** will not be sufficiently efficient to effectively dissociate the π - π dimer of hematin. Therefore, one molecule **2** might first associate on one side of the π - π dimer, thereby destabilizing it (e.g. marked variations of the broad and split Soret band, see Figure 8B). A second benzoxanthone molecule **2** can then intercalate within the weakened π - π dimer, leading to its dissociation and the formation a $[(\text{Fe}^{\text{III}}\text{PPIX})(\mathbf{2})_2]$ “sandwich” like complex in agreement with the loss of exciton coupling characterizing the hematin π - π dimer. The two complexes formed between hematin and benzoxanthone **2** were characterized by their electronic spectra (Figure 8B). With respect to $(\text{Fe}^{\text{III}}\text{PPIX})_2$ dimer, the $[(\text{Fe}^{\text{III}}\text{PPIX})_2(\mathbf{2})]$ species possesses a less intense, broad and split Soret band which is still confirming the dimeric nature of hematin. By contrast, $[(\text{Fe}^{\text{III}}\text{PPIX})(\mathbf{2})_2]$ displays a much sharper Soret band lying at lower energies ($\lambda_{\text{max}} = 401 \text{ nm}$, $\Delta\lambda = 18 \text{ nm}$ with respect to $(\text{Fe}^{\text{III}}\text{PPIX})_2$), in agreement with the dissociation of the hematin π - π dimer and the presence of a single $\text{Fe}^{\text{III}}\text{PPIX}$ heme surrounded by two benzoxanthones **2**. The thermodynamic and spectroscopic data are gathered in Table 3.

Xanthone **3** possesses similar association properties with hematin to benzoxanthone **1** and forms, under our experimental condition, a 1:1 complex associated to an apparent association constant of $\log K_{11} = 5.78 \pm 0.03$ ($K_D = 1.66 \mu\text{M}$). The $[(\text{Fe}^{\text{III}}\text{PPIX})(\mathbf{3})]$ species is characterized by a red shift of the hematin dimer Soret band to $\lambda_{\text{max}} \sim 399 \text{ nm}$. The introduction of two fluorine atoms also markedly modified the binding properties of xanthone **4** with hematin π - π dimer. The speciation behavior of compound **4** with hematin is indeed comparable to that of benzoxanthone **2** with two species being successively formed, namely the $[(\text{Fe}^{\text{III}}\text{PPIX})_2(\mathbf{4})]$ ($\log \beta_{21} = 11.4 \pm 0.1$, Equation 7) and $[(\text{Fe}^{\text{III}}\text{PPIX})(\mathbf{4})_2]$ ($\log \beta_{12} = 9.2 \pm 0.2$, Equation 9) species (Figure 9). Similar spectroscopic signatures can also be observed. $[(\text{Fe}^{\text{III}}\text{PPIX})_2(\mathbf{4})]$ is characterized by a broad and split Soret band in agreement with the π - π dimeric nature of heme, while the Soret absorption band of the $[(\text{Fe}^{\text{III}}\text{PPIX})(\mathbf{4})_2]$ species is much sharper and bathochromically shifted of 18 nm (Figure 9) with respect to $(\text{Fe}^{\text{III}}\text{PPIX})_2$ suggesting the presence of a single heme molecule encircled by two xanthone molecules. The successive apparent association constant of $[(\text{Fe}^{\text{III}}\text{PPIX})_2(\mathbf{4})]$ complex was calculated to be $\log K_{21} = 4.6$ ($K_D = 25.1 \mu\text{M}$, Equation 8) and is one order of magnitude lower than the association constants determined for the other substrates considered in this work. The introduction of fluorine atoms in the benzoxanthone or xanthone skeletons seemingly influence the electronic properties of these molecules and thereby disfavor efficient π - π interactions with the $\text{Fe}^{\text{III}}\text{PPIX}$ macrocycle. In addition, increasing bulkiness brought by these substituents likely play a critical role in the binding processes.

The xanthenes and benzoxanthenes considered in this work demonstrated their capacities to firmly interact with heme and to efficiently dissociate the $(\text{Fe}^{\text{III}}\text{PPIX})_2$ π - π dimer. In the context of hemozoin targeting, this property is of fundamental importance and is usually anticipated to be a first pre-requisite to allow interaction with hematin and subsequent inhibition of hemozoin formation. Introduction of fluorine or CF_3 substituents, however, alters the binding properties and leads to other stoichiometries such as 1:2 and 2:1 π - π complexes with hematin. The apparent association constants measured at pH 7.5 and at $T = 25 \text{ }^\circ\text{C}$ range from 5 to 6 (dissociation constants K_D in the μM range) and are comparable to those reported in the literature for antimalarial drug targeting hematin crystallization (Table 2). The main thermodynamic and spectroscopic results of the xanthone- and benzoxanthone-heme binding studies are gathered in Table 3.

1,4-Naphthoquinones—Based on a drug design and selection project, some of us recently demonstrated [18] that several benzyl-1,4-naphthoquinones were active at the nM concentrations against human pathogen *Plasmodium falciparum* in culture and against

Plasmodium berghei in infected mice. It was therefore of interest to examine the binding properties of two model 1,4-naphthoquinones **5** and **6** (Figure 6). The benzylnaphthoquinone **5** and the benzoylnaphthoquinone **6** display a similar speciation behavior with hematin (Figure 10). They both lead to 1:2 or 2:1 heme complexes, and are characterized by global association constants ranging from 10^{10} – 10^{13} M⁻² in 0.2 M sodium hepes buffer at pH 7.5 (Table 3). From the electronic spectra depicted in Figure 10B for the benzoylnaphthoquinone **6**, a substrate first aggregates with the dimeric unit of hematin to afford a stable 2:1 complex (successive association constant of $\log K_{21} = 5.6$, $K_D \sim 2.63$ μ M, Equation 8). The presence of a split and broad Soret band, but less intense, suggests that this heme species is not related to a “sandwich”-like arrangement but rather involve a substrate which is firmly associated on one face of the hematin π - π dimer (as already observed for several xanthenes and benzoxanthenes, vide supra). The strong absorptivity centered at about 350 nm originates from the phenolate subunit of substrate **6**. It is noteworthy that desolvation of at least one water molecule from an iron(III) center has to take place to allow π - π contacts between the heme (in the π - π dimeric state) and the substrate (i.e. the predominant iron(III) protoporphyrinic species at pH 7.5 is $[(\text{Fe}^{\text{III}}\text{PPIX}(\text{OH}_2))_2(\text{Fe}^{\text{III}}\text{PPIX}(\text{OH}))]$). Addition of excess of the substrate will favor the formation of a 2:1 species with one protoporphyrin core being encircled by two substrates as suggested by the sharp and strong bathochromic shift ($\Delta\lambda = 17$ nm) of the Soret band (Figure 10). The loss of the charge transfer at ~ 610 nm is also indicative of the presence of a single heme unit within $[(\text{Fe}^{\text{III}}\text{PPIX})(\text{S})_2]$ complexes.

Our spectroscopic and thermodynamic approach demonstrate the ability of xanthenes, benzoxanthenes or 1,4-naphthoquinones to strongly interact (K_D in the μ M scale, see Table 3) with hematin π - π dimer and to lead to its dissociation *via* the formation of $[(\text{Fe}^{\text{III}}\text{PPIX})(\text{S})]$ or $[(\text{Fe}^{\text{III}}\text{PPIX})(\text{S})_2]$ complexes. These apparent association values measured at pH 7.5 are comparable to those reported in the literature for the most efficient antimalarial agents, such as chloroquine or quinine, which were shown to efficiently target and prevent hemozoin biocrystallization (Table 2). In the next section, we will evaluate the potential of these compounds to inhibit β -hematin crystallization under quasi-physiological conditions (concentration, temperature, pH...) which mimic the acidic digestive vacuoles and guts of the *Plasmodium* parasites and *Schistosoma* worms, respectively. The aim of this study is to correlate the heme binding properties of our substrates to inhibition of hemozoin formation.

Inhibition of β -Hematin Formation

Principle of the Assay

The host's hemoglobin digestion by *Plasmodium* parasites and *Schistosoma* worms leads to the accumulation of free toxic heme. The parasites detoxify this exogenous deleterious species through biomineralization processes leading to an insoluble and much less active crystal named hemozoin. Inhibition of heme oligomerization would lead to death of the parasite by accumulation of toxic free heme in the membranes and subsequent oxidative stress [56,73]. Many antiparasitic agents against blood-feeding parasites were consequently designed to target the heme biocrystallization process. After a first evaluation of the heme binding capacities of our compounds, we then undertook a biochemical investigation of our compounds as inhibitors of hematin crystallization to β -hematin, the synthetic equivalent of hemozoin. We used a biochemical assay previously developed by K. K. Ncokazi and T. J. Egan [74]. This assay, performed first at a pH of ca. 5–5.5 (i.e. pH of the digestive vacuole at which hemozoin biomineralization efficiently occurs), is based on a classical hematin quantification method known as the pyridine ferrihemochrome method [75]. Aqueous pyridine (used in a very large excess – 5% by volume) forms a hexacoordinated low-spin complex with free heme $[(\text{Fe}^{\text{III}}\text{PPIX})(\text{Pyr})_2]$, but not with β -hematin. This red colored complex has a very high absorptivity of the Soret band in the visible region ($\epsilon^{405} = 1.04 \times$

$10^5 \text{ M}^{-1} \text{ cm}^{-1}$, Figure 11). Therefore, it allows a straightforward quantification of the residual free hematin in the presence of our substrates as reporter activity for inhibition of the hematin oligomerization (carried out at pH about 4.5–5.0). The final pH value of the assay was 7.5 after addition of the buffers containing pyridine (0.2 M sodium hepes + 5% (v/v) pyridine buffer at pH 8.2 and 0.02 M sodium hepes + 5% pyridine (v/v) buffer at pH 7.5) used to stop the reaction. The experimental conditions optimized by T. J. Egan and his coworkers were modified for our compounds (order of the addition of the reagents) and our assays were monitored by UV-visible absorption spectrophotometry (absorption spectra recorded from 300 nm to 750 nm). IC_{50} values for inhibition of β -hematin formation were determined from the absorbance changes at 405 nm *versus* the drug (equiv.) / hematin (equiv.) ratio in the following plots (*vide infra*).

Xanthenes and Benzoxanthenes—The four xanthone and benzoxanthone derivatives were evaluated for their ability to inhibit β -hematin crystallization. Despite their ability to strongly interact with hematin (Table 3), all these compounds displayed no significant inhibitory activity of hematin crystallization and displayed similar spectral variations to those depicted as examples in Figure 12 for benzoxanthone **1** and xanthone **3**. The maximum of inhibition reached for the four xanthenes or benzoxanthenes is about 20–30% at 5 equivalents which can be clearly interpreted as the absence of any inhibitory potential for hematin crystallization of these substrates. Indeed, these inhibition values are usually reached for control experiments at 0 mM drug concentration. In addition, nor the addition of the drug simultaneously to hematin prior incubation at 60°C for one hour (typical conditions used to prepare β -hematin, see section above), neither the addition of the drug to preformed β -hematin led to significantly inhibitory activities. These data clearly demonstrate that these xanthone and benzoxanthone derivatives did not display any inhibitory potential for hematin crystallization either by prevention or by dissociation. To further confirm that most of the antimalarial drugs mainly prevent β -hematin formation rather than dissociating it, we carried out inhibition assays with amodiaquine under identical conditions. As expected, amodiaquine prevents β -hematin formation while it possesses weaker capacity to dissociate pre-formed β -hematin crystals as shown in Figure 13.

Figure 14 displays the IR spectral characteristics of β -hematin crystals in the absence (Figure 14A) and in the presence of benzoxanthone **1** (Figure 14B) and of xanthone **3** (Figure 14D). Infrared spectroscopy was herein used to characterize the reaction products and to provide further information about the inhibitory activities of compounds **1–4** with respect to β -hematin. This technique unambiguously distinguishes between hematin and β -hematin [58]. The latter has distinct and intense sharp bands at 1661 and 1204 cm^{-1} which are absent in the former. Three equivalents of benzoxanthone **1** (Figure 14B) or of xanthone **3** (Figure 14D) did not inhibit the reaction in agreement with the previous β -hematin inhibition data. No drug association with hematin can be also demonstrated since the IR peaks of xanthone derivatives **1** or **3** observed in combination with β -hematin possess identical characteristics as in the absence of β -hematin. These data demonstrate that even though benzoxanthenes **1** and **2** and xanthenes **3** and **4** are able to bind to ferriprotoporphyrin, they do exhibit any inhibitory activity toward β -hematin. π - π interactions are mainly expected to drive the complex formation which is by far not sufficient to prevent β -hematin formation as observed, for instance, for arylmethanols antimalarials such as quinine, mefloquine or halofantrine [12,47].

1,4-Naphthoquinones—By contrast with the xanthone- and benzoxanthone-based substrates, the benzyl-1,4-naphthoquinone **5** and the benzoyl-1,4-naphthoquinone **6** displayed significant inhibitory potential to hinder β -hematin formation. The benzyl-naphthoquinone **5** was shown to inhibit the formation of β -hematin by a maximum of 80%

at a drug (equiv.) / hematin (equiv.) ratio of 5. The IC_{50} value which was accordingly determined is equal to 4.2 drug equiv./ hematin equiv. (Figure 15). Among the substrates examined in this work, the benzoyl-naphthoquinone **6** is by far the most efficient system which efficiently prevents the formation of β -hematin ($IC_{50} = 1.3$ drug (equiv.) / hematin (equiv.) with a maximum of inhibition of 90 %, Figure 15).

The main results of the hematin crystallization inhibition by xanthenes and benzoxanthenes are gathered in Table 4. It clearly appears from the binding studies and the inhibition of β -hematin formation assays that no clear and direct correlation exists. For our systems, their capacities to prevent formation of the β -hematin (or hemozoin) are therefore not only related to their ability to firmly interact with the π - π hematin dimer (used as a model of β -hematin and hemozoin). Consequently, the mechanism by which the formation of hemozoin is prevented is most likely induced by another process. To get further insight into this mechanism of action, we then examined the ability of our substrates to reduce heme-containing targets in the presence of disulfide reductases.

Spectroscopic and Kinetic Studies of the Reduction of Methemoglobin to Hemoglobin

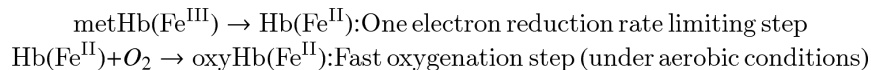
Principle of the assay

Plasmodium parasites and *Schistosoma* worms use methemoglobin (hereafter noted metHb(Fe^{III})) as a source of aminoacids for their own growth and digest it faster than hemoglobin (hereafter noted oxyHb(Fe^{II})). At pH 5.0 to 6.0 (acidic digestive vacuoles or guts of *Plasmodium* parasites and *Schistosoma* worms, respectively), hemoglobin (Hb Fe^{II}) or oxyhemoglobin (oxyHb or oxyHb(Fe^{II})) is quickly oxidized to methemoglobin (metHb or metHb(Fe^{III})). Consequently, the reduction of metHb(Fe^{III}) to oxyHb(Fe^{II}) can significantly slow down methemoglobin digestion.

The ability of our compounds to inhibit disulfide reductases (*P. falciparum* GR – noted *pGR*- and of human erythrocytes – noted *hGR* or *S. mansoni* – noted *SmTGR*) combined to their potency to reduce metHb(Fe^{III}) to oxyHb(Fe^{II}) (or heme-containing targets) could contribute to rise oxidative stress and interfere with hemozoin formation; both phenomena possibly leading to the death of the parasites. The pernicious and continuous use of NADPH flux under the catalysis of these disulfide reductases in the presence of our redox-active compounds (which behave as substrates or electron acceptors) can dramatically increase the flux of toxic reduced species (hydronaphthoquinones in the case of starting naphthoquinones; leucomethylene blue from methylene blue) within the parasite and lead to its death by shifting the equilibrium (Fe^{III}) to (Fe^{II}) heme species. In addition, efficient reduction of the other ferric centers of porphyrinic targets such as hematin π - π dimers can also significantly contribute to the prevention of hemozoin (or β -hematin) crystallization.

In order to evaluate the potency of our compounds to reduce metHb(Fe^{III}) to oxyHb(Fe^{II}), we used a reduction assay coupled to the *hGR*/NADPH system *in vitro* which regenerate the reduced species of our substrates continuously. This assay was recently established as a relevant *in vivo* model in our laboratory [18]. The UV-visible absorption spectrum of metHb(Fe^{III}) between 300 nm and 700 nm is characterized by a maximum absorbance centered at 405 nm (Soret band of the Fe^{III} heme and a broad band centered at 603 nm, see *vide supra*). Upon metHb(Fe^{III}) reduction by our redox-active compounds ($T = 37^{\circ}C$; pH = 6.9), which were pre-reduced by *hGR*, the formation of the oxyHb(Fe^{II}) species is associated to a bathochromic shift of the maximum of absorption of the Soret band from 405 nm to about 410 nm (in fact it corresponds to oxyHb(Fe^{II}) with the metal cation being

hexacoordinated in a low spin state, see *vide supra*), as well as the formation of two new less intense absorptions at ~ 536 nm and ~ 576 nm.



No shift of the absorption band centered at 405 nm and, consequently, no metHb(Fe^{III}) reduction was observed in the presence of chloroquine, used as negative control [18]. No shift of the Soret band was also observed in the absence of the redox-active drugs (control experiment, *vide infra*), demonstrating that hGR/NADPH-base system is not the prevailing reducing system and confirming that the substrates, under their reduced states, correspond to the bioactive intermediates during the reduction of metHb(Fe^{III}) into oxyHb(Fe^{II}) mediated by the glutathione reductase. The spectral changes as well as the kinetic parameters of the reduction reaction were thoroughly analyzed. Since the coupled assay based on metHb(Fe^{III}) and the hGR/NADPH-based system was performed with all the compounds under identical experimental conditions, the apparent kinetic rates can be compared and discussed and picture the redox-cycling capacities of the xanthone, benzoxanthone and 1,4-naphthoquinone substrates.

Xanthenes and Benzoxanthenes—The four members of the xanthone and benzoxanthone series, whose binding capacities with hematin and inhibition properties of β -hematin formation were described (*vide supra*), were evaluated for their ability to reduce methemoglobin Fe(III) into hemoglobin Fe(II) (in fact oxyHb(Fe^{II})) in the coupled assay with glutathione reductase and NADPH (used as cofactor). Even though all these four compounds were found to strongly interact with hematin π - π dimer at pH 7.5 and $T = 25$ °C in water, most of them did not induce a significant and fast reduction of metHb(Fe^{III}) into oxyHb(Fe^{II}) (pH = 6.9, $T = 37$ °C). Benzoxanthenes **1** and **2** were not capable to reduce metHb(Fe^{III}) and the very weak shift observed, if any, was no more than 1 nm. In addition, assays of metHb(Fe^{III}) reduction performed with benzoxanthenes **1** and **2** display similar spectrophotometric characteristics as illustrated in Figure 16. The decrease of absorption band at 340 nm can be ascribed to NADPH consumption by the GR, while the weak decrease of the absorption of the Soret band is most likely related to degradation of metHb(Fe^{III}) [77].

According to the absorption spectra recorded within the timescale (one hour) which was considered, xanthenes **3** and **4** apparently do not induce fast reduction of metHb(Fe^{III}) into oxyHb(Fe^{II}). The processing of the absorption data set *versus* time, however, allowed us to evidence the presence of two rate-limiting steps, with the second one being most likely associated to a slow reduction process of metHb(Fe^{III}) into oxyHb(Fe^{II}) (i.e. (i) a shift of only 2 nm of the Soret band takes place after one hour in the presence of **3** and **4**; (ii) a new and weak absorption band at ~ 540 nm is gradually formed with time; Figure 17a). As previously suggested for benzoxanthenes **1** and **2**, the first step may correspond to slow degradation of metHb(Fe^{III}), while the second slower one is associated to the substrate-mediated reduction of metHb(Fe^{III}). We calculated the apparent first order rate constants related to both steps. For the metHb(Fe^{III}) reduction rate limiting step, the k_{obs} values are equal to $k_{\text{obs}} = (7 \pm 2) \times 10^{-5} \text{ s}^{-1}$ for **3** ($t_{\text{red}}^{1/2} = 165$ min) and $k_{\text{obs}} = (1.2 \pm 0.2) \times 10^{-4} \text{ s}^{-1}$ for **4** ($t_{\text{red}}^{1/2} = 96.3$ min).

In contrast with benzoxanthenes **1** and **2**, xanthenes **3** and **4** are capable of reducing metHb(Fe^{III}) into oxyHb(Fe^{II}) but according to very slow processes ($t_{\text{red}}^{1/2} \approx 1.5 - 3$ h) which are by far not biological relevant. These data show that, even though these xanthone

and benzoxanthone derivatives are able to interact with hemein π - π dimer in water at pH 7.5 (Table 3), only those with fine-tuned electrochemical characteristics would rapidly and efficiently reduce metHb(Fe^{III}) into oxyHb(Fe^{II}), an important pre-requisite when targeting inhibition of hemozoin formation, redox homeostasis and death of the parasites. In the other hand, this weak capacity to efficiently and rapidly reduce metHb(Fe^{III}) can be seemingly related to their inability to inhibit β -hemein formation. The major results of the spectroscopic and kinetic studies relative to the metHb(Fe^{III}) reduction coupled-assay with hGR/NADPH with the benzoxanthenes **1** and **2** and the xanthenes **3** and **4** are summarized in Table 5.

1,4-Naphthoquinones—The benzyl- **5** and the benzoylnaphthoquinone **6** were then evaluated for their ability to reduce metHb(Fe^{III}) into oxyHb(Fe^{II}) in the coupled assay with human glutathione reductase and NADPH. After pre-reduction (two electrons reduction process) with hGR/NADPH-based system under aerobic conditions [18], the dihydrogenated form of naphthoquinones **5** and **6** induce, in a much faster step ($t_{1/2}^{\text{red}} = 5\text{--}6$ min), a significant bathochromic shift of the Soret band ($\sim 3\text{--}5$ nm) of the metHb(Fe^{III}) Soret transitions within the time range considered (20 to 45 min). These two compounds were shown to behave similarly as depicted in the UV-visible spectra provided in Figure 18. For example, a red shift from 405 to 410 nm was observed during the first rate-limiting step for compound **6** ($k_{\text{obs}} = (2.07 \pm 0.03) \times 10^{-3} \text{ s}^{-1}$, $t_{1/2}^{\text{red}} = 5.55$ min). For most of these substrates, slower steps (Figure 19) were also observed but concern either re-oxidation or degradation of oxyHb(Fe^{II}) once hGR/NADPH becomes inactive (i.e. when NADPH is consumed or when hGR becomes inactive). The kinetic and spectroscopic results obtained for the metHb(Fe^{III}) reduction by substrates **5** and **6** are provided in Table 5.

Figure 19 illustrates the major mediation role of the hGR/NADPH system on the metHb(Fe^{III}) reduction by our redox-cyclers (mainly 1,4-naphthoquinone substrates). Methemoglobin is stable in solution at pH 6.9 as depicted in Figure 19A and NADPH, which is the cofactor of hGR, has no influence on its reduction (Figure 19B). When mixing metHb(Fe^{III}) with the 3-benzoyl-1,4-naphthoquinone **6** in the absence of hGR/NADPH (Figure 19C), no reduction occurs as well. Mixing metHb(Fe^{III}) in the presence of the hGR/NADPH system, but in the absence of the redox-cycler **6**, has also no effect on the reduction of metHb(Fe^{III}). Disulfide reductases, such as the human glutathione reductase (hGR), are therefore not able by themselves to efficiently reduce these ferric targets. Importantly, the presence of hGR and its cofactor NADPH pre-reduced the redox-cycler substrate which is then able to trigger in its turn the reduction of metHb(Fe^{III}) into oxyHb(Fe^{II}). These spectroscopic data enlightened that the bioactive forms of the substrates are the reduced species and clearly pointed out the crucial role of glutathione reductase in mediating metHb(Fe^{III}) reduction by pre-reducing the substrate.

The thorough examination of the data obtained for the six substrates (Table 4 and Table 5) strikingly indicates that the redox-cyclers which are capable of efficiently reducing the metHb(Fe^{III}) into oxyHb(Fe^{II}) are also those which are able to inhibit β -hemein (or hemozoin) formation, thus suggesting a closely related mode of action. Since all the compounds tested in this study were shown to interact with hemein π - π dimer (used as a model), no direct correlation can be establish between the ability to bind heme and bioactivity of these compounds toward the parasites, as it is usually anticipated for other series of drugs. However, our substrates (used as representative models of xanthone, benzoxanthone and 1,4-naphthoquinone redox-cyclers) operate according to a new mode of action which mainly targets the reduction of Fe(III)-containing species such as methemoglobin, ferric protoporphyrin or hemozoin-type biocrystals. The mechanism by which the inhibition of hemozoin (or β -hemein) is induced by these redox substrates is not related to the ability of the drugs to prevent hemozoin or β -hemein formation, but rather to

their capacity to reduce the ferriprotoporphyrinic units, thereby weakening the hemozoin or β -hematin packing interactions. Their ability to rapidly and efficiently induce methemoglobin reduction in presence of disulfide reductases can also drastically slow down methemoglobin digestion by the parasites and will contribute to their overall bioactivities and to the prevention of the pathogen development.

Conclusion

In this study, we combined complementary bioanalytical methods such as absorption spectrophotometric binding titrations, hematin crystallization assay and methemoglobin reduction assay to evaluate the strength of the interactions between xanthone-, benzoxanthone- and 1,4-naphthoquinone-based substrates with the iron(III)-containing targets hematin and methemoglobin in solution under quasi-physiological conditions. These physico-biochemical data allowed us to identify the key parameters related to the mechanism of action of redox substrates toward parasitic pathogens (*Plasmodium* and *Schistosoma*). All substrates were shown to firmly interact with hematin π - π dimer in hepes buffer at pH 7.5, which is frequently predicted to be a first prerequisite when targeting hemozoin formation. It appears from our studies that the capacity of our redox-active compounds to rapidly and efficiently reduce methemoglobin has also to be taken into account to rationalize their potential in preventing or inhibiting β -hematin (or hemozoin) formation. The inhibition of β -hematin crystallization was evaluated and correlated well to the binding properties and electron transfer capacities of our substrates.

Six low solubility-featured compounds which possess structures conferring high antiparasitic properties, namely the 1,4-naphthoquinone and the xanthone series, revealed valuable information for the better understanding of their mechanisms of action.

All the compounds were shown to display high affinities for hematin and lead to either 1:1 or 1:2 (and 2:1) charge-transfer complexes with apparent dissociation constant in the μ M range (0.2 M sodium hepes buffer at pH 7.5). These binding constants are comparable to those reported for the major antimalarial drugs (Table 2) targeting hemozoin formation and demonstrate the propensity of our substrates to efficiently dissociate the hematin π - π dimer in model solutions. This binding study allowed us to draw structure-activity relationships such as substitution pattern, nature of the substituent, bulkiness of the substrate and redox properties. Even though all the tested substrates interact with hematin π - π dimer, only few of them displayed a potent inhibitory activity in the hematin crystallization assay. In contrast to some previous reports, no direct correlation between a high affinity for hematin π - π dimer and the capacity to prevent β -hematin formation can be deduced.

The ability of our substrates to reduce methemoglobin to hemoglobin was thus examined and discussed in the frame of β -hematin formation. Once again, only few compounds were shown to efficiently and rapidly reduce methemoglobin(Fe^{III}) to hemoglobin(Fe^{II}). Very interestingly, a direct correlation between methemoglobin reduction and inhibition of hematin crystallization was observed, thereby demonstrating that the two processes are closely related. Compounds displaying an ability to reduce methemoglobin are also very potent inhibitors of β -hematin formation. The facility of our redox-active agents (mainly the naphthoquinone series) to be rapidly and efficiently reduced by NADPH with mediation of the disulfide reductases (i.e. glutathione reductase) and, in their reduced forms, to catalytically and specifically transfer electrons to ferric species of heme and hemoglobin contribute to interference with hemozoin biomineralization. Both events – oxidizing the reductants and reducing the oxidants in a continuous redox cycle – are expected to lead to the death of the parasites. These multifaceted properties of these hematin binders, efficient methemoglobin reductants after bio-reduction by NADPH/GR couple and potent inhibitors of

hemozoin/ β -hematin oligomerization of several representatives of the naphthoquinone and xanthone/benzoxanthone series will guide the design and the synthesis of redox active antimalarial and antischistosomal drugs with optimized properties.

Experimental Section

Physico-Biochemical Studies

Materials and Methods—Distilled water was purified by passing it through a mixed bed of ion-exchanger (Bioblock Scientific R3-83002, M3-83006) and activated carbon (Bioblock Scientific ORC-83005). All stock solutions were prepared using an AG 245 Mettler Toledo analytical balance. The $[\text{Fe}^{\text{III}}\text{PPIX}]_{\text{tot}}$ and $[\text{metHb}(\text{Fe}^{\text{III}})]_{\text{tot}}$ were calculated from the molecular weight of the corresponding monomers. Hepes (2-[4-(2-hydroxyethyl)piperazin-1-yl]ethanesulfonic acid, Gerbu Biotechnik) buffer (0.2 M) was prepared in water and the pH (7.4) was adjusted with NaOH slurry. pH reading was done on a PHM240 MeterLab® millivoltmeter fitted with a combined glass electrode (Metrohm 6.0234.500, Long Life, 0.1 M NaCl). Calibration was done with commercial Merck® buffers (1.68, 4.00, 6.86, 7.41, and 9.18). Stock solutions of the substrates in DMSO for the different assays were freshly prepared in Eppendorf tubes just before the experiments. Hematin ($\text{Fe}^{\text{III}}\text{PPIX}(\text{OH})$) solution was prepared from hemin equine Type III ($\text{Fe}^{\text{III}}\text{PPIXCl}$, Sigma-Aldrich) and 0.1 M NaOH solution vigorously stirred at room temperature (RT) for 1 h. Methemoglobin was prepared by oxidation of Human hemoglobin (Sigma-Aldrich) in solution by oxygen at RT (the molecular weight of the tetrameric hemoglobin is 64.458 kDa). NADPH (Biomol, Hambourg, Germany) solution was prepared in water and kept at 0°C during the experiments. The final concentration in the optical cell was calculated from the absorbance at 340 nm ($\epsilon_{340} = 6.22 \text{ mM}^{-1} \text{ cm}^{-1}$).

Spectrophotometric titration of hematin π - π dimer by the substrates: An aliquot of 10 μL of the $\text{Fe}^{\text{III}}\text{PPIX}(\text{OH})$ stock solution ($\sim 1.68 \text{ mM}$) were dissolved in 500 μL 0.2 M sodium hepes buffer at pH 7.5 in a 1 cm Hellma optical cell. The absorption spectrophotometric titrations were carried out by adding microvolumes of a stock solution of the substrate ($\sim 5\text{--}9 \times 10^{-4} \text{ M}$ in DMSO). Aliquots of 5–20 μL of the stock substrate solution were successively added to the reaction mixture and, after each addition, a UV-visible absorption spectrum (300 nm $<\lambda < 800$ nm) was recorded with a Uvikon 941 spectrophotometer. Special care was taken to ensure that equilibrium was attained. The association constants K_A and the stoichiometries of the species at equilibrium were determined by processing the spectrophotometric data with the Specfit program [67,68,69,70,71,72]. Specfit uses factor analysis to reduce the absorbance matrix and to extract the eigenvalues prior to the multiwavelength fit of the reduced data set according to the Marquardt algorithm. The uncertainties on the log K values are given as 3σ with $\sigma =$ standard deviation. Distribution curves of the various complexes and protonated species were calculated using the Hyss 2006 program [78]. Origin 5.0 was used to process the analytical results [79]. For the sake of simplicity charges are omitted in all the chemical equilibria.

β -Hematin Inhibition Assay: The β -hematin inhibition assay used in this work was inspired from that developed by the group of T. J. Egan [74] with some significant improvements in the order of the addition of the reactants, which was imposed by the low solubility of some of our compounds. Drug solutions (89.1 mM, 53.5 mM, 26.7 mM, 17.8 mM, 13.4 mM, 8.9 mM, 4.5 mM, 0 mM) were prepared by dissolving the drug in DMSO (Table 6). Hematin stock solution (1.68 mM) was prepared by dissolving equine hemin (1.05 mg) in 0.1 M NaOH (960 μL). The solution was incubated at room temperature for 1 h. In a series of 2 mL Eppendorf tubes, 2.0 μL of drug solution (or solvent for the blank

reference) were dispensed. Then, 20.2 μL of hematin stock solution were added. The Eppendorf tubes were placed in an incubator at 60°C and then, 2 μL of 1 M HCl and 11.7 μL of 12.9 M sodium acetate solution (pH 4.5) pre-incubated at 60°C were added. The final hematin concentration was 1 mM. The final drug concentrations were 4.96 mM, 2.98 mM, 1.45 mM, 0.99 mM, 0.75 mM, 0.5 mM, 0.25 mM and 0 mM and the final pH of the solution was 4.5. The reaction mixtures were incubated at 60°C for 1 h. After incubation, the reaction mixtures were quenched at room temperature by adding 900 μL of 0.2 M sodium hepes buffer + 5% (v/v) pyridine (pH 8.2), to adjust the final pH of the mixture to a value between 7.2 and 7.5. Then, 1100 μL of 0.02 M sodium hepes buffer + 5% pyridine (v/v) (pH 7.5) was added. The Eppendorf tubes were shaken and the precipitate of β -hematin was scrapped from the walls of the Eppendorf tubes to ensure complete dissolution of hematin. The β -hematin was allowed to settle at room temperature for 1 h. The supernatant was carefully transferred to a Hellma optical cell ($l = 1$ cm) without disturbing the precipitate and the absorption spectra were measured between 300 and 750 nm.

MetHb reduction assay

Enzyme: Recombinant *hGR* was purified as previously reported [80]. One unit of GR activity is defined as the consumption of 1 μmol NADPH per min under conditions of substrate saturation. The enzyme stock solution (266 μM) used for kinetic determinations were > 98% pure as judged from silver stained SDS-PAGE and had specific activities of 200 U/mg (*hGR*). A *hGR* stock II solution was prepared by dilution (1/10) of the enzyme stock solution with *hGR* buffer (pH 6.9). [18]. The *hGR* buffer (pH 6.9) was prepared by dissolving KH_2PO_4 (2.79 g), K_2HPO_4 , 3 H_2O (6.04 g), EDTA (0.372 g), and KCl (14.91 g) in 1 L water. The pH was adjusted by dropwise addition of 5 M KOH.

Methemoglobin Reduction Coupled Assay with *hGR*/NADPH: Stock solutions of 2 mM of the drugs in DMSO were freshly prepared. Solutions of 397 μM methemoglobin in *hGR* buffer and ca. 4 mM NADPH in water were prepared and kept at 0°C during the experiment. The final NADPH concentration in the optical cell was calculated from the absorbance at 340 nm ($\epsilon_{340} = 6.22 \text{ mM}^{-1} \text{ cm}^{-1}$). In a Hellma optical cell ($l = 1$ cm), 945 μL of the *hGR* buffer, 20 μL of the methemoglobin solution (397 μM), 20 μL of the drug solution (2 mM) and 10 μL of the NADPH solution (ca. 4 mM) were introduced and pre-incubated at 37.5°C (Lauda E200/O11 thermostat and a Huber Minichiller cooler) for 5 min. Then, 5 μL of the *hGR* stock II solution was added. The reaction was monitored by UV-vis. absorption spectrophotometry on a Cary 300 spectrophotometer with the scanning kinetics method. A spectrum was measured every 30s between 250 and 500 nm over 1 to 2 h. The kinetic data were processed with the Specfit program [67,68,69,70,71,72].

Synthesis

Materials and Methods—Melting points were determined on a Büchi melting point apparatus and were not corrected. ^1H (300 MHz), ^{13}C (75 MHz) and ^{19}F (282 MHz) NMR spectra were recorded on a Bruker DRX-300 spectrometer; chemical shifts were expressed in ppm relative to tetramethylsilane (TMS); multiplicity is indicated as s (singlet), d (doublet), t (triplet), q (quartet), sep (septet), m (multiplet), cm (centered multiplet), dd (doublet of a doublet), dt (doublet of a triplet), and td (triplet of a doublet). C_q indicates a quaternary carbon in the ^{13}C NMR assignment. ^{19}F NMR was performed using 1,2-difluorobenzene as external standard ($\delta = -139.0$ ppm). IR spectra (cm^{-1}) were recorded on a Perkin–Elmer Spectrum One Spectrophotometer. Intensities in the IR spectra are indicated as vs (very strong), s (strong), m (medium), w (weak), and b (broad). Elemental analyses were carried out at the Mikroanalytisches Laboratorium der Chemischen Fakultät der Universität Heidelberg. Electron impact mass spectrometry (EI-MS) was recorded at facilities of the Institut für Organische Chemie der Universität Heidelberg. Analytical TLC

was carried out on pre-coated Sil G-25 UV₂₅₄ plates from Macherey&Nagel. Flash chromatography was performed using silica gel G60 (230–400 mesh) from Macherey&Nagel.

Synthesis of Xanthenes 1 to 4

General Procedure 1: A flask was purged with Argon and the following reagents were successively introduced under inert atmosphere: the arene (2.0 equiv.), the benzonitrile (1.0 equiv.), Pd(OAc)₂ (0.1 equiv.), DMSO and TFA (Scheme 3 and Scheme 4). The flask was sealed and the reaction mixture was stirred and heated at 95°C for 24 h. The mixture was cooled and 8 mL of water was added to the flask. The resulting mixture was heated at 70°C for 2 h. Then, the mixture was cooled and extracted three times with 15 mL Et₂O. The combined organic layers were dried over MgSO₄ and evaporated. The resulting oil was purified through flash chromatography.

(2,5-dimethoxyphenyl)(2-fluorophenyl)methanone (3a): Commercially available 1,4-dimethoxybenzene (500 mg, 3.62 mmol), 2-fluorobenzonitrile (220 mg, 1.81 mmol), DMSO (0.20 mL) and TFA (4.5 mL) were used as starting materials and treated according to general procedure. The resulting yellow oil was purified through flash chromatography (hexane:EtOAc 2:1). The product **3a** was obtained as a colorless oil (400 mg, 1.54 mmol, 85%). R_f (hexane:EtOAc 2:1) = 0.44. ¹H NMR (300 MHz, CDCl₃): δ (ppm) = 7.76–7.85 (m, 2H), 7.61–7.73 (m, 1H), 7.34–7.45 (m, 2H), 7.19–7.25 (m, 1H), 7.05 (d, *J* = 8.79 Hz, 1H), 3.95 (s, 3H, OCH₃), 3.77 (s, 3H, OCH₃). ¹³C NMR (75 MHz, CDCl₃): δ (ppm) = 193.71 (C=O), 161.03 (d, ¹*J*_{CF} = 256 Hz, C_q-F), 153.41 (C_q), 153.05 (C_q), 133.94 (d, ³*J*_{CF} = 9 Hz, CH_{ar}), 130.95 (d, ⁴*J*_{CF} = 2 Hz, CH_{ar}), 129.11 (C_q), 128.0 (d, ²*J*_{CF} = 12 Hz, C_q), 124.09 (d, ³*J*_{CF} = 3.7 Hz, CH_{ar}), 120.00 (CH_{ar}), 115.96 (d, ²*J*_{CF} = 22 Hz, CH_{ar}), 114.75 (CH_{ar}), 113.29 (CH_{ar}), 56.24 (OCH₃), 55.92 (OCH₃). ¹⁹F NMR (282 MHz, CDCl₃): δ (ppm) = -112.81 (ddd, ³*J*_{HF} = 11 Hz, ⁴*J*_{HF} = 7 Hz, ⁴*J*_{HF} = 5 Hz). EI-MS (70 eV, *m/z* (%)): 260.2 ([M⁺], 100) for C₁₅H₁₃FO₃ [64].

(2-fluorophenyl)(2-hydroxy-5-methoxyphenyl)methanone (3b): A solution of (2,5-dimethoxyphenyl)(2-fluorophenyl)methanone **3a** (100 mg, 0.384 mmol) in 8 mL of dichloromethane (DCM) was cooled at 0°C and kept stirring for 30 min. Then, BBr₃ (0.38 mL, 1M in DCM) was added dropwise to the solution and the reaction mixture was stirred at 0°C for 1 h. The reaction mixture was quenched with 8 mL of methanol (MeOH). A saturated solution of NaCl was added to the mixture and it was extracted three times with 10 mL DCM and twice with 10 mL ethyl acetate. The organic layers were combined, dried over MgSO₄ and evaporated. The product **3b** was obtained as a yellow powder (82 mg, 0.33 mmol, 86%). R_f (cyclohexane:DCM 3:2) = 0.32. ¹H NMR (300 MHz, CDCl₃): δ (ppm) = 11.59 (s, 1H, Ph-OH), 7.45–7.58 (m, 2H, H_{ar}), 7.14–7.32 (m, 3H, H_{ar}), 7.01 (d, *J* = 9.1 Hz, 1H, H_{ar}), 6.86 (t, *J* = 7.5 Hz, 1H, H_{ar}), 3.68 (s, 3H, OCH₃). ¹³C NMR (75 MHz, CDCl₃): δ (ppm) = 198.10 (C=O), 159.10 (d, ¹*J*_{CF} = 252 Hz, C_q-F), 157.54 (C_q), 151.77 (C_q), 132.96 (d, ³*J*_{CF} = 8 Hz, CH_{ar}-F), 129.87 (d, ³*J*_{CF} = 8 Hz, CH_{ar}-F), 126.21 (d, ²*J*_{CF} = 16 Hz, C_q-F), 125.02 (CH_{ar}), 124.40 (CH_{ar}), 119.31 (C_q), 119.19 (CH_{ar}), 116.37 (d, ²*J*_{CF} = 21 Hz, CH_{ar}-F), 115.17 (d, ⁴*J*_{CF} = 2 Hz, CH_{ar}-F), 55.90 (OCH₃). ¹⁹F NMR (282 MHz, CDCl₃): δ (ppm) = -112.22 (cm, ³*J*_{HF} = 10 Hz, ⁴*J*_{HF} = 7 Hz, ⁴*J*_{HF} = 5 Hz, ⁵*J*_{HF} = 3 Hz). EI-MS (70 eV, *m/z* (%)): 246.1 ([M⁺], 100) for C₁₄H₁₁FO₃ [64].

(2,4-difluoro-6-hydroxy-3-methoxyphenyl)(2-fluorophenyl)methanone (4a): Commercially available 4-methoxy-3,5-difluorophenol (200 mg, 1.25 mmol), 2-fluorobenzonitrile (67 μL, 0.63 mmol), DMSO (0.06 mL) and TFA (1.6 mL) were used as starting materials and treated according to general the procedure 1. The resulting brown oil was purified through flash chromatography (cyclohexane:EtOAc 10:1). The product **4a** was obtained as a yellow powder (25 mg, 0.09 mmol, 14%). R_f (cyclohexane:EtOAc 10:1) = 0.34. ¹H NMR (300

MHz, CDCl₃): δ (ppm) = 11.93 (s, 1H, Ph-OH), 7.50–7.57 (m, 2H), 7.27 (ddd, $^3J_{\text{HH}} = 8$ Hz, $^4J_{\text{HF}} = 7$ Hz, $^4J_{\text{HH}} = 1$ Hz, 1H), 7.13 (ddd, $^3J_{\text{HF}} = 10$ Hz, $^3J_{\text{HH}} = 8$ Hz, $^4J_{\text{HH}} = 1$ Hz, 1H), 6.61 (dd, $^3J_{\text{HF}} = 12$ Hz, $^5J_{\text{HF}} = 2$ Hz, 1H), 3.85 (s, 3H, OCH₃). ¹³C NMR (75 MHz, CDCl₃): δ (ppm) = 193.70 (C=O), 164.90 (C_q), 161.62 (dd, $^1J_{\text{CF}} = 259$ Hz, $^3J_{\text{CF}} = 9$ Hz, C_q-F), 161.24 (C_q), 159.57 (d, $^1J_{\text{CF}} = 252$ Hz, C_q-F), 156.81 (dd, $^1J_{\text{CF}} = 259$ Hz, $^3J_{\text{CF}} = 9$ Hz, C_q-F), 159.23 (dd, $^2J_{\text{CF}} = 16$ Hz, C_q-O), 156.36 (C_q), 133.57 (d, $^3J_{\text{CF}} = 8$ Hz, CH_{ar}), 129.38 (d, $^3J_{\text{CF}} = 8$ Hz, CH_{ar}), 124.40 (d, $^4J_{\text{CF}} = 3$ Hz, CH_{ar}), 115.84 (d, $^2J_{\text{CF}} = 22$ Hz, CH_{ar}), 101.50 (dd, $^2J_{\text{CF}} = 22$ Hz, $^4J_{\text{CF}} = 3$ Hz, CH_{ar}), 62.49 (t, $^4J_{\text{CF}} = 3$ Hz, OCH₃). ¹⁹F NMR (282 MHz, CDCl₃): δ (ppm) = -113.87 (dd, $^4J_{\text{FF}} = 15$ Hz, $^3J_{\text{HF}} = 12$ Hz), -114.47 (cm, $^3J_{\text{HF}} = 13$ Hz, $^4J_{\text{HF}} = 7$ Hz), -122.21 (dd, $^4J_{\text{FF}} = 15$ Hz, $^5J_{\text{HF}} = 7$ Hz). EI-MS (70 eV, m/z (%)): 282.1 ([M⁺], 24) for C₁₄H₉F₃O₃.

General procedure 2: The benzophenone derivative (1.0 equiv.) and K₂CO₃ (2.0 equiv.) were placed in a round-bottom flask. The flask was sealed under Argon and 10 mL of dry Acetone were added. The reaction mixture was stirred at 50°C for 2 h. The suspension was then filtered through a pad of celite and washed with 25 mL of diethylether (Et₂O). The filtrate was concentrated under vacuum.

2-methoxy-9H-xanthen-9-one (3): (2-fluorophenyl)(2-hydroxy-5-methoxyphenyl)methanone **3b** (80 mg, 0.325 mmol) was used as a starting material and treated according to general procedure 2. The 2-methoxy-9H-xanthen-9-one (**3**) was obtained as white, “cotton-like” flakes (45 mg, 0.20 mmol, 61%). R_f (cyclohexane:DCM 3:2) = 0.20. ¹H NMR (300 MHz, CDCl₃): δ (ppm) = 8.35 (dd, $^3J = 8$ Hz, $^4J = 1$ Hz, 1H), 7.69–7.75 (m, 2H), 7.31–7.50 (m, 4H), 3.92 (1H, 3H, OCH₃). ¹³C NMR (75 MHz, CDCl₃): δ (ppm) = 177.09 (C=O), 156.14 (C_q-O), 156.02 (C_q), 151.02 (C_q), 134.60 (CH_{ar}), 126.69 (CH_{ar}), 124.91 (CH_{ar}), 123.73 (CH_{ar}), 122.14 (C_q), 121.27 (C_q), 119.43 (CH_{ar}), 113.23 (CH_{ar}), 105.86 (CH_{ar}), 55.95 (CH₃). EI-MS (70 eV, m/z (%)): 226.1 ([M⁺], 42), 211.1 ([M-CH₃]⁺, 30) for C₁₄H₁₀O₃. Elemental analysis calcd for C₁₄H₁₀O₃ (%): C, 74.33; H, 4.46; found: C, 74.04; H, 4.38. m.p. 126–128°C.

2,4-difluoro-3-methoxy-9H-xanthen-9-one (4): (2,4-difluoro-6-hydroxy-3-methoxyphenyl)(2-fluorophenyl)methanone **4a** (200 mg, 0.71 mmol) was used as a starting material and treated according to general procedure 2. 2,4-difluoro-3-methoxy-9H-xanthen-9-one (**4**) was obtained as a beige powder (100 mg, 0.38 mmol, 53%). R_f (cyclohexane:EtOAc 10:1) = 0.21. ¹H NMR (300 MHz, CDCl₃): δ (ppm) = 8.30 (dd, $^3J = 8$ Hz, $^4J = 1$ Hz, 1H), 7.72 (dd, $^3J = 8$ Hz, $^4J = 1$ Hz, 1H), 7.40–7.45 (m, 2H), 7.06 (dd, $^3J_{\text{HF}} = 10$ Hz, $^5J_{\text{HF}} = 2$ Hz, 1H), 4.04 (1H, 3H, OCH₃); ¹³C NMR (75 MHz, CDCl₃): δ (ppm) = 174.53 (C=O), 159.61 (C_q), 158.94 (C_q), 159.46 (dd, $^1J_{\text{CF}} = 260$ Hz, $^3J_{\text{CF}} = 8$ Hz, C_q-F), 155.37 (C_q), 154.99 (dd, $^1J_{\text{CF}} = 257$ Hz, $^3J_{\text{CF}} = 8$ Hz, C_q-F), 151.96 (dd, $^3J_{\text{CF}} = 16$ Hz, C_q), 134.92 (CH_{ar}), 126.68 (CH_{ar}), 124.50 (CH_{ar}), 121.75 (C_q), 117.47 (CH_{ar}), 101.35 (dd, $^2J_{\text{CF}} = 23$ Hz, $^4J_{\text{CF}} = 4$ Hz, CH_{ar}), 62.47 (dd, $^4J_{\text{CF}} = 3$ Hz, OCH₃). ¹⁹F NMR (282 MHz, CDCl₃): δ (ppm) = -116.61 (dd, $^4J_{\text{FF}} = 15$ Hz, $^3J_{\text{HF}} = 11$ Hz), -126.69 (d, $^4J_{\text{FF}} = 15$ Hz). EI-MS (70 eV, m/z (%)): 262.0 ([M⁺], 73), 247.0 ([M-CH₃]⁺, 15). Elemental analysis calcd for C₁₄H₁₀O₃ (%): C, 64.13; H, 3.08; found: C, 64.36; H, 3.02. m.p. 125–127°C.

Characterization Data of Benzoxanthenes 1 and 2: 5-methoxy-6-methyl-7H-benzo[c]xanthen-7-one (1) was obtained as an orange powder (96 mg, 0.33 mmol, 69%). R_f (cyclohexane:EtOAc 10:1) = 0.36. ¹H NMR (300 MHz, CDCl₃): δ (ppm) = 8.61–8.64 (m, 1H), 8.31–8.34 (m, 1H), 8.13–8.16 (m, 1H), 7.69–7.75 (m, 2H), 7.58–7.65 (m, 2H), 7.37–7.42 (cm, 1H), 3.91 (s, 3H, OCH₃), 2.96 (s, 3H, CH₃). ¹³C NMR (75 MHz, CDCl₃): δ (ppm) = 178.68 (C=O), 154.81 (C_q), 151.84 (C_q), 149.81 (C_q), 133.93 (CH_{ar}), 130.99 (C_q), 129.87 (CH_{ar}), 126.57 (CH_{ar}), 126.29 (CH_{ar}), 125.86 (C_q), 124.22 (CH_{ar}), 123.79 (C_q), 123.28 (CH_{ar}), 123.21 (C_q), 122.17 (CH_{ar}), 117.46 (CH_{ar}), 117.35 (C_q), 61.45 (OCH₃),

14.51 (CH₃). EI-MS (70 eV, m/z (%)): 290.1 ([M⁺], 53) for C₁₉H₁₄O₃. Elemental analysis calcd for C₁₉H₁₄O₃ (%): C, 78.61; H, 4.86; found: C, 78.81; H, 4.92. m.p. 175–177°C.

5-methoxy-6-methyl-11-(trifluoromethyl)-7H-benzo[c]xanthen-7-one (2) was obtained as a light yellow, cotton-like solid (120 mg, 0.33 mmol, 86%). ¹H NMR (300 MHz, CDCl₃): δ (ppm) = 8.66–8.68 (m, 1H), 8.54–8.57 (m, 1H), 8.17–8.20 (m, 1H), 8.02–8.05 (m, 1H), 7.76–7.82 (cm, 1H), 7.67–7.73 (cm, 1H), 7.47–7.53 (cm, 1H), 3.92 (s, 3H, OCH₃), 2.97 (s, 3H, CH₃). ¹³C NMR (75 MHz, CDCl₃): δ (ppm) = 177.39 (C=O), 151.79 (C_q), 151.52 (C_q), 150.50 (C_q), 131.27 (q, ³J_{CF} = 4 Hz, CH_{ar}), 130.99 (CH_{ar}), 130.30 (CH_{ar}), 126.92 (CH_{ar}), 125.56 (C_q), 124.05 (C_q), 123.70 (C_q), 123.49 (CH_{ar}), 123.34 (CH_{ar}), 123.13 (q, ¹J_{CF} = 273 Hz, CF₃), 122.15 (CH_{ar}), 119.70 (C_q), 119.08 (q, ²J_{CF} = 32 Hz, C_q-CF₃), 117.32 (C_q), 61.54 (OCH₃), 14.46 (CH₃). ¹⁹F NMR (282 MHz, CDCl₃): δ (ppm) = –61.31 (s, CF₃). EI-MS (70 eV, m/z (%)): 358.0 ([M⁺], 60), 343.0 ([M-CH₃]⁺, 100) for C₂₀H₁₃O₃F₃. Elemental analysis calcd for C₂₀H₁₃O₃F₃ (%): C, 67.04; H, 3.66; found: C, 66.95; H, 3.80. m.p. 198–200°C.

Acknowledgments

The Centre National de la Recherche Scientifique (CNRS) and the University of Strasbourg (UMR 7509 CNRS-UdS) partly supported this work. This work was also funded by the International Center for Frontier Research in Chemistry (ic-FRC) in Strasbourg. L.J. and D.A.L. are grateful to DFG *via* the SFB 544 (B14 project) and NIH/National Institute of Allergy and Infectious Disease (NIAID) (grant R01AI065622) for their salaries. The authors are grateful to Sokune Seng for her help in measuring IR spectra and β-hematin inhibition assay.

List of Abbreviations

<i>e</i>	molar absorptivity coefficient
benzoxanthone	benz[c]xanthen-7-one
<i>λ</i>	wavelength
CT	charge transfer (complex or band)
DCM	dichloromethane
DMSO	dimethylsulfoxide
EDTA	ethylenediaminetetraacetic acid
EI-MS	electron impact mass spectrometry
Fe^{III}PPIX	ferriprotoporphyrin
Fe^{III}PPIXCl	ferriprotoporphyrin chloride
Hb(Fe^{II})	hemoglobin subunit
<i>h</i>GR	human glutathione reductase
<i>K</i>_A	association constant
<i>K</i>_D	dissociation constant
<i>K</i>_{Dim}	dimerization constant
M	molar
MeOH	methanol
metHb(Fe^{III})	methemoglobin subunit
NADPH	reduced form of nicotinamide adenine dinucleotide phosphate
oxyHb(Fe^{II})	hemoglobin subunit with O ₂ molecule coordinated on iron(II)

ROS	reactive oxygen species
TFA	trifluoroacetic acid
tot	total
UV-vis	ultraviolet/visible (spectroscopy)

References

1. Corrêa Soares JB, Maya-Monteiro CM, Bittencourt-Cunha PR, Atella GC, Lara FA, d'Avila JC, Menezes D, Vannier-Santos MA, Oliveira PL, Egan TJ, Oliveira MF. Extracellular lipid droplets promote hemozoin crystallization in the gut of the blood fluke *Schistosoma mansoni*. *FEBS Lett*. 2007; 581:1742–50. [PubMed: 17418143]
2. Oliveira MF, d'Avila JC, Torres CR, Oliveira PL, Tempone AJ, Rumjanek FD, Braga CM, Silva JR, Dansa-Petretski M, Oliveira MA, de Souza W, Ferreira ST. Haemozoin in *Schistosoma mansoni*. *Mol Biochem Parasitol*. 2000; 111:217–21. [PubMed: 11087932]
3. Chen MM, Shi L, Sullivan DJ Jr. *Haemoproteus* and *Schistosoma* synthesize heme polymers similar to *Plasmodium* hemozoin and beta-hematin. *Mol Biochem Parasitol* 2001; 113:1–8. b) Egan, TJ, Recent advances in understanding the mechanism of hemozoin (malaria pigment) formation. *J Inorg Biochem* 2008; 102: 1288–99. c) Weissbuch, I, Leiserowitz, L. Interplay between malaria, crystalline hemozoin formation, and antimalarial drug action and design. *Chem Rev*. 2008; 108:4899–914. [PubMed: 19006402]
4. Schirmer RH, Müller JG, Krauth-Siegel RL. Disulfide reductase inhibitors as chemotherapeutic agents: the design of drugs for trypanosomiasis and malaria. *Angew Chem Int Ed*. 1995; 34:141–54.
5. Krauth-Siegel RL, Bauer H, Schirmer RH. Dithiol proteins as guardians of the intracellular redox milieu in parasites: old and new drug targets in trypanosomes and malaria-causing plasmodia. *Angew Chem Int Ed*. 2005; 44:690–715.
6. a) Atamna H, Ginsburg H. Heme degradation in the presence of glutathione. A proposed mechanism to account for the high levels of non-heme iron found in the membranes of hemoglobinopathic red blood cells. *J Biol Chem*. 1995; 270:24876–83. [PubMed: 7559611] b) Meierjohan S, Walter RD, Müller S. Regulation of intracellular glutathione levels in erythrocytes infected with chloroquine-sensitive and chloroquine-resistant *Plasmodium falciparum*. *Biochem J*. 2002; 368:761–8. [PubMed: 12225291]
7. Färber PM, Arscott LD, Williams CH Jr, Becker K, Schirmer RH. Recombinant *Plasmodium falciparum* glutathione reductase is inhibited by the antimalarial dye methylene blue. *FEBS Lett* 1998; 422: 311–4. b) Buchholz K, Schirmer RH, Eubel JK, Akoachere MB, Dandekar T, Becker K, Gromer S. Interactions of methylene blue with human disulfide reductases and their orthologues from *Plasmodium falciparum*. *Antimicrob Agents Chemother* 2008; 52: 183–91. c) Davioud-Charvet E, Delarue S, Biot C, Schwöbel B, Böhme CC, Müssigbrodt A, Maes L, Sergheraert C, Grellier P, Schirmer RH, Becker K. A prodrug form of a *Plasmodium falciparum* glutathione reductase inhibitor conjugated with a 4-anilinoquinoline. *J Med Chem*. 2001; 44:4268–76. [PubMed: 11708927]
8. Alger HM, Williams DL. The disulfide redox system of *Schistosoma mansoni* and the importance of a multifunctional enzyme, thioredoxin glutathione reductase. *Mol Biochem Parasitol*. 2002; 121:129–39. [PubMed: 11985869]
9. Kuntz AN, Davioud-Charvet E, Dessolin J, Sayed AA, Califf LL, Arnér ESJ, Williams DL. Schistosome redox balance and thioredoxin glutathione reductase: An essential parasite enzyme and novel drug target. *PLoS Medicine*. 2007; 4:e206, 1–16. Erratum in: *PLoS Medicine* 2007; 4: e264. [PubMed: 17579510]
10. Oliveira MF, d'Avila JC, Tempone AJ, Soares JB, Rumjanek FD, Ferreira-Pereira A, Ferreira ST, Oliveira PL. Inhibition of heme aggregation by chloroquine reduces *Schistosoma mansoni* infection. *J Infect Dis*. 2004; 190:843–52. [PubMed: 15272414]
11. Corrêa Soares JB, Menezes D, Vannier-Santos MA, Ferreira-Pereira A, Almeida GT, Venancio TM, Verjovski-Almeida S, Zishiri VK, Kuter D, Hunter R, Egan TJ, Oliveira MF. Interference

- with hemozoin formation represents an important mechanism of schistosomicidal action of antimalarial quinoline methanols. *PLoS Negl Trop Dis*. 2009; 3:e477. [PubMed: 19597543]
12. de Villiers KA, Marques HM, Egan TJ. The crystal structure of halofantrine-ferriprotoporphyrin IX and the mechanism of action of arylmethanol antimalarials. *J Inorg Biochem*. 2008; 102:1660–7. [PubMed: 18508124]
 13. Xiao SH, Catto BA. In vitro and in vivo studies of the effect of artemether on *Schistosoma mansoni*. *Antimicrob Agents Chemother* 1989; 33: 1557–62. b) Hong YL, Yang YZ, Meshnick SR. The interaction of artemisinin with malarial hemozoin. *Mol Biochem Parasitol* 1994; 63: 121–8. c) Klayman DL. Qinghaosu (artemisinin): an antimalarial drug from China. *Science*. 1985; 228:1049–55. [PubMed: 3887571]
 14. a) Xu Kelly J, Winter R, Riscoe M, Peyton DH. A spectroscopic investigation of the binding interactions between 4,5-dihydroxyxanthone and heme. *J Inorg Biochem*. 2001; 86:617–25. [PubMed: 11566335] b) Nabih I. Structure and activity in the schistosomicidal thioxanthone and xanthone derivatives. *J Pharm Sci*. 1966; 55:221–2. [PubMed: 5923279]
 15. Ignatushchenko MV, Winter RW, Bächinger HP, Hinrichs DJ, Riscoe MK. Xanthenes as antimalarial agents; studies of a possible mode of action. *FEBS Lett*. 1997; 409:67–73. [PubMed: 9199506]
 16. Riscoe M, Kelly JX, Winter R. Xanthenes as antimalarial agents: discovery, mode of action, and optimization. *Curr Med Chem*. 2005; 12:2539–49. [PubMed: 16250876]
 17. McMillan PJ, Stimmler LM, Foth BJ, McFadden GI, Müller S. The human malaria parasite *Plasmodium falciparum* possesses two distinct dihydrodipyrromethane dehydrogenases. *Mol Microbiol*. 2005; 55:27–38. [PubMed: 15612914]
 18. Müller T, Johann L, Jannack B, Brückner M, Lanfranchi DA, Bauer H, Sanchez C, Yardley V, Deregnacourt C, Schrével J, Lanzer M, Schirmer RH, Davioud-Charvet E. Glutathione reductase-catalyzed cascade of redox reactions to bioactivate potent antimalarial 1,4-naphthoquinones - A new strategy to combat malarial parasites. *J Am Chem Soc*. 2011; 133:11557–71. [PubMed: 21682307]
 19. Davioud-Charvet, E.; Lanfranchi, DA. Subversive substrates of glutathione reductases from *P. falciparum*-infected red blood cells as antimalarial agents. In: Becker, K.; Selzer, PM., editors. *Apicomplexan parasites -Molecular approaches toward targeted drug development*. Vol. 2. Wiley-VCH Verlag GmbH & Co. KGaA; Weinheim: 2011. from the series *Drug Discovery in Infectious Diseases*
 20. Asher C, de Villiers KA, Egan TJ. Speciation of ferriprotoporphyrin IX in aqueous and mixed aqueous solution is controlled by solvent identity, pH, and salt concentration. *Inorg Chem*. 2009; 48:7994–8003. [PubMed: 19572726]
 21. Ncokazi KK, Egan TJ. A colorimetric high-throughput beta-hematin inhibition screening assay for use in the search for antimalarial compounds. *Anal Biochem*. 2005; 338:306–19. [PubMed: 15745752]
 22. Monti D, Vodopivec B, Basilico N, Oliaro P, Taramelli D. A novel endogenous antimalarial: Fe(II)-protoporphyrin IX alpha (heme) inhibits hematin polymerization to beta-hematin (malaria pigment) and kills malaria parasites. *Biochemistry*. 1999; 38:8858–63. [PubMed: 10413458]
 23. Hogg T, Nagarajan K, Herzberg S, Chen L, Shen X, Jiang H, Wecke M, Blohmke C, Hilgenfeld R, Schmidt CL. Structural and functional characterization of Falcipain-2, a hemoglobinase from the malarial parasite *Plasmodium falciparum*. *J Biol Chem*. 2006; 281:25425–37. [PubMed: 16777845]
 24. Anstey NM, Hassanali MY, MLalasi J, Manyenga D, Mwaikambo ED. Elevated levels of methaemoglobin in Tanzanian children with severe and uncomplicated malaria. *Trans R Soc Trop Med Hyg*. 1996; 90:147–51. [PubMed: 8761575]
 25. Blank O, Davioud-Charvet E, Elhabiri M. Interactions of the antimalarial methylene blue with methemoglobin and heme derivatives - A physico-biochemical study. *Antioxid & Redox Signal*. 2012; 17:544–554.
 26. Lehane AM, Hayward R, Saliba KJ, Kirk K. A verapamil-sensitive chloroquine-associated H⁺ leak from the digestive vacuole in chloroquine-resistant malaria parasites. *J Cell Sci*. 2008; 121:1624–32. [PubMed: 18445688]

27. Ryter SW, Tyrell RM. The heme synthesis and degradation pathways: Role in oxidant sensitivity. *Free Radic Biol Med.* 2000; 28:289–309. [PubMed: 11281297]
28. Schmitt TH, Frezzatti WA Jr, Schereier S. Heme-induced lipid membrane disorder and increased permeability: a molecular model for the mechanism of cells lysis. *Arch Biochem Biophys.* 1993; 307:96–103. [PubMed: 8239671]
29. Oliveira MF, Timm BL, Machado EA, Miranda K, Attias M, Silva JR, Dansa-Petretski M, de Oliveira MA, de Souza W, Pinhal NM, Sousa JJ, Vugman NV, Oliveira PL. On the pro-oxidant effects of haemozoin. *FEBS Lett.* 2002; 512:139–44. [PubMed: 11852068]
30. Green MD, Xiao L, Lal AA. Formation of hydroxyeicosatetraenoic acids from hemozoin-catalyzed oxidation of arachidonic acid. *Mol Biochem Parasitol.* 1996; 83:183–8. [PubMed: 9027751]
31. Schwarzer E, Bellomo G, Giribaldi G, Ulliers D, Arese P. Phagocytosis of malarial pigment haemozoin by human monocytes: a confocal microscopy study. *Parasitology.* 2001; 123:125–31. [PubMed: 11510677]
32. Hanscheid T, Egan TJ, Grobusch MP. Haemozoin: from melatonin pigment to drug target, diagnostic tool, and immune modulator. *Lancet Infect Dis.* 2007; 7:675–85. [PubMed: 17897610]
33. Cheng L, Lee J, Powell DR, Richter-Addo GB. μ -Oxo-bis[(protoporphyrin IX dimethyl ester)-iron(III)]. *Acta Crystallogr, Sect E: Struct Rep Online.* 2004; 60:m1340–m1342.
34. Koenig DF. The structure of α -chlorohemin. *Acta Crystallogr.* 1965; 18:663–73. [PubMed: 14287744]
35. a) Pagola S, Stephens PW, Bohle DS, Kosar AD, Madsen SK. The structure of malaria pigment β -haematin. *Nature.* 2000; 404:307–10. [PubMed: 10749217] b) Bohle DS, Dodd EL, Kosar AJ, Sharma L, Stephens PW, Suárez L, Tazoo D. Soluble synthetic analogues of malaria pigment: structure of mesohematin anhydride and its interaction with chloroquine in solution. *Angew Chem Int Ed.* 2011; 50:6151–4.
36. Shack J, Clarke WM. Metalloporphyrins: VI. Cycles of changes in systems containing heme. *J Biol Chem.* 1947; 171:143–87.
37. Brown SB, Dean TC, Jones P. Aggregation of ferrihaems. Dimerization and protolytic equilibria of protoferrihaem and deuteroferrihaem in aqueous solution. *Biochem J.* 1970; 117:733–9. [PubMed: 5449127]
38. Little RG, Dymock KR, Ibers JA. Crystal and molecular structure of the ferrihemochrome bis(1-methylimidazole)(protoporphyrin IX)iron-methanol-water. *J Am Chem Soc.* 1975; 97:4532–9. [PubMed: 1159221]
39. de Villiers KA, Kaschula CH, Egan TJ, Marques HM. Speciation and structure of ferriprotoporphyrin IX in aqueous solution: Spectroscopic and diffusion measurements demonstrate dimerization, but not μ -oxo dimer formation. *J Biol Inorg Chem.* 2007; 12:101–17. [PubMed: 16972088]
40. Crespo MP, Tilley L, Klonis N. Solution behavior of hematin under acidic conditions and implications for its interactions with chloroquine. *J Biol Inorg Chem.* 2010; 15:1009–22. [PubMed: 20429019]
41. Klonis N, Dilanian R, Hanssen E, Darmanin C, Streltsov V, Deed S, Quiney H, Tilley L. Hematin-hematin self-association states involved in the formation and reactivity of the malaria parasite pigment, hemozoin. *Biochemistry.* 2010; 49:6804–11. [PubMed: 20593810]
42. Das DK, Medhi OK. The role of heme propionate in controlling the redox potentials of hemes: square wave voltammetry of protoporphyrinato IX iron(III) in aqueous surfactant micelles. *J Inorg Biochem.* 1998; 70:83–90. [PubMed: 9666570]
43. a) Slater AF, Swiggard WJ, Orton BR, Flitter WD, Goldberg DE, Cerami A, Henderson GB. An iron-carboxylate bond links the heme units of malaria pigment. *Proc Natl Acad Sci.* 1991; 88:325–29. [PubMed: 1988933] b) Fitch CD, Kanjanangulpan P. The state of ferriprotoporphyrin IX in malaria pigment. *J Biol Chem.* 1987; 262:15552–5. [PubMed: 3119578]
44. Egan TJ, Chen JYJ, de Villiers KA, Mabothe TE, Naidoo KJ, Ncokazi KK, Langford SJ, McNaughton D, Pandiancherri S, Wood BR. Haemozoin (β -haematin) biomineralization occurs by self-assembly near the lipid/water interface. *FEBS Lett.* 2006; 580:5105–10. [PubMed: 16956610]
45. a) Egan TJ, Hunter R, Kaschula CH, Marques HM, Mispion A, Walden JC. Structure-function relationships in aminoquinolines: effect of amino and chloro groups on quinoline-hematin

- complex formation, inhibition of beta-hematin formation, and antiplasmodial activity. *J Med Chem.* 2000; 43:283–91. [PubMed: 10649984] b) Kuter D, Chibale K, Egan TJ. Linear free energy relationships predict coordination and π -stacking interactions of small molecules with ferriprotoporphyrin IX. *J Inorg Biochem.* 2011; 105:684–92. [PubMed: 21450272]
46. Ogoshi, H.; Mizutani, T.; Hayashi, T.; Kuroda, Y. *The Porphyrin Handbook.* Kadish, KM.; Smith, KM.; Guilard, R., editors. Vol. 6. Academic Press; San Diego, CA: 2000.
47. de Villiers KA, Egan TJ. Recent advances in the discovery of haem-targeting drugs for malaria and schistosomiasis. *Molecules.* 2009; 14:2868–87. [PubMed: 19701131]
48. Burrows JN, Chibale K, Wells TNC. The state of the art in anti-malarial drug discovery and development. *Curr Top Med Chem.* 2011; 11:1226–54. [PubMed: 21401508]
49. Atamna H, Krugliak M, Shalmiev G, Deharo E, Pescarmona G, Ginsburg H. Mode of antimalarial effect of methylene blue and some of its analogues on *Plasmodium falciparum* in culture and their inhibition of *P. vinckei petteri* and *P. yoelii nigeriensis* *in vivo*. *Biochem Pharmacol* 1996; 51: 693–700. b) Kalkanidis M, Klonis N, Tilley L, Deady LW. Novel phenothiazine antimalarials: synthesis, antimalarial activity, and inhibition of the formation of beta-haematin. *Biochem Pharmacol.* 2002; 63:833–42. [PubMed: 11911834]
50. a) Egan TJ, Mavuso WW, Ncokazi KK. The mechanism of beta-hematin formation in acetate solution. Parallels between hemozoin formation and biomineralization processes. *Biochemistry.* 2001; 40:204–13. [PubMed: 11141072] b) Egan TJ. Haemozoin formation as a target for the rational design of new antimalarials. *Drug Design Rev.* 2004; 1:93–110.
51. Egan TJ, Mavuso WW, Ross DC, Marques HM. Thermodynamic factors controlling the interaction of quinoline antimalarial drugs with ferriprotoporphyrin IX. *J Inorg Biochem.* 1997; 68:137–45. [PubMed: 9336973]
52. Loria P, Miller S, Foley M, Tilley L. Inhibition of the peroxidative degradation of haem as the basis of action of chloroquine and other quinoline antimalarials. *Biochem J.* 1999; 339:363–70. [PubMed: 10191268]
53. a) Egan TJ. Haemozoin (malaria pigment): a unique crystalline drug target. *Targets.* 2003; 2:115–24. b) Egan TJ, Ncokazi KK. Quinoline antimalarials decrease the rate of β -hematin formation. *J Inorg Biochem.* 2005; 99:1532–9. [PubMed: 15927260]
54. Egan TJ. Interactions of quinoline antimalarials with hematin in solution. *J Inorg Biochem.* 2006; 100:916–26. [PubMed: 16384600]
55. Winter RW, Ignatushchenko M, Ogundahunsi OAT, Cornell KA, Oduola AMJ, Hinrichs DJ, Riscoe MK. Potentiation of an antimalarial oxidant drug. *Antimicrob Agents Chemother.* 1997; 41:1449–54. [PubMed: 9210664]
56. Kelly JX, Winter R, Riscoe MK, Peyton DH. A spectroscopic investigation of the binding interactions between 4,5-dihydroxanthone and heme. *J Inorg Biochem.* 2001; 86:617–25. [PubMed: 11566335]
57. Bachhawat K, Thomas CJ, Surolia N, Surolia A. Interaction of chloroquine and its analogues with heme: an isothermal titration calorimetric study. *Biochem Biophys Res Commun.* 2000; 276:1075–79. [PubMed: 11027592]
58. Egan TJ, Hempelmann E, Mavuso WW. Characterisation of synthetic β -haematin and effects of the antimalarial drugs quinidine, halofantrine, desbutylhalofantrine and mefloquine on its formation. *J Inorg Biochem.* 1999; 73:101–7. [PubMed: 10212997]
59. Dascombe MJ, Drew MGB, Morris H, Wilairat P, Auparakkitanon S, Moule WA, Alizadeh-Shekalgourabi S, Evans PG, Lloyd M, Dyas AM, Carr P, Ismael FMD. Mapping antimalarial pharmacophores as a useful tool for the rapid discovery of drugs effective *in vivo*: design construction, characterisation and pharmacology of mefloquine. *J Med Chem.* 2005; 48:5423–36. [PubMed: 16107142]
60. Dorn A, Vippagunta SR, Matile H, Jaquet C, Vennerstrom JL, Ridley RG. An assessment of drug-haematin binding as a mechanism for inhibition of haematin polymerisation by quinoline antimalarials. *Biochem Pharmacol.* 1998; 55:727–36. [PubMed: 9586944]
61. Biot C, Taramelli D, Forfar-Bares I, Maciejewski LA, Boyce M, Nowogrocki G, Brocard JS, Basilico N, Olliaro P, Egan TJ. Insights on the mechanism of action of ferroquine. Relationship between physicochemical properties and antimalarial activity. *Mol Pharmaceut.* 2005; 2:185–93.

62. Dubar F, Egan TJ, Pradines B, Kuter D, Ncokazi KK, Forge D, Paul JF, Pierrot C, Kalamou H, Khalife J, Buisine E, Rogier C, Vezin H, Forfar I, Slomianny C, Trivelli X, Kapishnikov S, Leiserowitz L, Dive D, Biot C. The antimalarial ferroquine: role of the metal and intramolecular hydrogen bond in activity and resistance. *ACS Chem Biol.* 2011; 6:275–87. [PubMed: 21162558]
63. Sousa ME, Pinto MMM. Synthesis of xanthenes: an overview. *Curr Med Chem.* 2005; 12:2447–79. [PubMed: 16250872]
64. Zhou C, Larock RC. Synthesis of aryl ketones or ketimines by palladium-catalyzed arene C-H addition to nitriles. *J Org Chem.* 2006; 71:3551–8. [PubMed: 16626140]
65. Yoshida S, Iizuka T, Nozawa T, Hatano M. Studies on the charge transfer band in high spin state of ferric myoglobin and hemoglobin by low temperature optical and magnetic circular dichroism spectroscopy. *Biochim Biophys Acta (BBA) - Protein Structure.* 1975; 405:122–35.
66. Eaton WA, Hanson LK, Stephens PJ, Sutherland JC, Dunn JBR. Optical spectra of oxy- and deoxyhemoglobin. *J Am Chem Soc.* 1978; 100:4991–5003.
67. Gampp H, Maeder M, Meyer CJ, Zuberbühler AD. Calculation of equilibrium constants from multiwavelength spectroscopic data-I Mathematical considerations. *Talanta.* 1985; 32:95–101. [PubMed: 18963802]
68. Rossoti FJC, Rossoti HS, Whewell RJ. The use of electronic computing techniques in the calculation of stability constants. *J Inorg Nucl Chem.* 1971; 33:2051–65.
69. Gampp H, Maeder M, Meyer CJ, Zuberbühler AD. Calculation of equilibrium constants from multiwavelength spectroscopic data - II. SPECFIT: Two user-friendly programs in BASIC and standard FORTRAN 77. *Talanta.* 1985; 32:257–64. [PubMed: 18963840]
70. Gampp H, Maeder M, Meyer CJ, Zuberbühler AD. Calculation of equilibrium constants from multiwavelength spectroscopic data - IV. Model-free least-squares refinement by use of evolving factor analysis. *Talanta.* 1986; 33:943–51. [PubMed: 18964236]
71. Marquardt DW. An algorithm for least-squares estimation of nonlinear parameters. *J Soc Indust Appl Math.* 1963; 11:431–41.
72. Maeder M, Zuberbühler AD. Nonlinear least-squares fitting of multivariate absorption data. *Anal Chem.* 1990; 62:2220–4.
73. Vippagunta SR, Dorn A, Matile H, Bhattacharjee AK, Karle JM, Ellis WY, Ridley RG, Vennerstrom JL. Structural specificity of chloroquine-hematin binding related to inhibition of hematin polymerization and parasite growth. *J Med Chem.* 1999; 42:4630–9. [PubMed: 10579825]
74. Ncokazi KK, Egan TJ. A colorimetric high-throughput beta-hematin inhibition screening assay for use in the search for antimalarial compounds. *Anal Biochem.* 2005; 338:306–19. [PubMed: 15745752]
75. a) Partos S. The hemochrome of Herzfeld and Klinger. *Biochem Zeit.* 1922; 129:89–100. b) Marques HM, Munro OQ, Crawcour ML. Coordination of N-donor ligands by hemochrome. *Inorg Chim Acta.* 1992; 196:221–9.
76. Egan TJ, Ross DC, Adams PA. Quinoline anti-malarial drugs inhibit spontaneous formation of π -haematin (malaria pigment). *FEBS Letters.* 1994; 352:54–7. [PubMed: 7925942]
77. Kelder PP, De Molt NJ, Lamberth MJ. Mechanistic aspects of the oxidation of phenothiazine derivatives by methemoglobin in the presence of hydrogen peroxide. *Biochem Pharmacol.* 1991; 42:1551–9. [PubMed: 1930282]
78. Alderighi L, Gans P, Ienco A, Peters D, Sabatini A, Vacca A. Hyperquad simulation and speciation (HySS): a utility program for the investigation of equilibria involving soluble and partially soluble species. *Coord Chem Rev.* 1999; 184:311–8.
79. MicrocalTM OriginTM. Microcal Software, Inc; Northampton, MA: 1997.
80. Nordhoff A, Bucheler US, Werner D, Schirmer RH. Folding of the four domains and dimerization are impaired by the Gly446→Glu exchange in human glutathione reductase. Implications for the design of antiparasitic drugs. *Biochemistry.* 1993; 32:4060–6. [PubMed: 8097111]

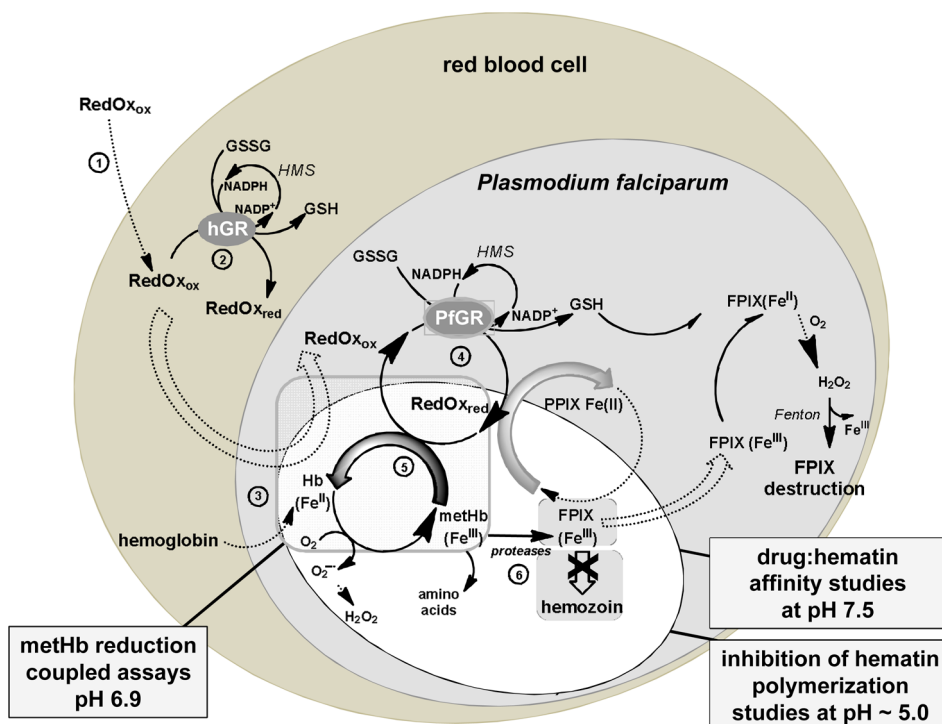
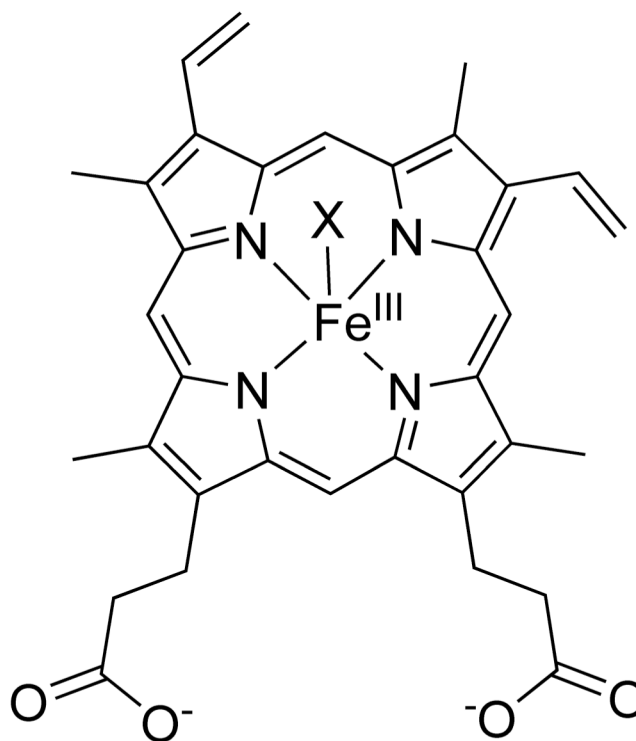


Figure 1. Putative Model for Redox-Active Compounds Affecting Redox Homeostasis in *P. falciparum*-Infected Red Blood Cell Accounting for the Observed Inhibition of Hemozoin Formation Causing the Death of the Parasites.^a

^aHMS, hexose monophosphate shunt. RedOx means redox-active compound with ox and red in subscript to indicate if the compound acts in its oxidized or its reduced state. Double dashed arrows represent transport processes. The potential redox-active compounds are proposed to be taken up by the infected red blood cells (step 1), to be reduced in the cytosol of the human red blood cell by GR (step 2), and then transported in the acidic vesicles or in the food vacuole (step 3) where hemoglobin digestion occurs. Subsequently, the redox-active compounds are proposed to be cycled between the acidic compartments and the cytosols and reduced by GR of the human host cell (not shown) or of the parasite (step 4) in a continuous redox cycle. The reduced species of redox-active compounds are assumed to be transported through Fe^{III} complexation into the acidic vesicles where the reduced RedOx species transfer the electrons to oxidants (hematin or metHb(Fe^{III}), step 5). The final result is an inhibition of hemozoin formation (step 6) and the arrest of trophozoite development. Thus, the physico-biochemical properties of RedOx accounting for the antimalarial activity were investigated through the different processes under quasi-physiological conditions in the presence of relevant parasitic oxidant targets like hematin or metHb(Fe^{III}). Three assays are described: drug:hematin affinity studies at pH 7.5; inhibition of hematin crystallization at pH ~ 5.0; metHb(Fe^{III}) reduction assays at pH 6.9 coupled to the NADPH-based GR system.



Fe^{III} PPIX

hemin

X=Cl⁻

hematin

X= H₂O/HO⁻

Figure 2.
Chemical Structure of the Deprotonated Form of Fe^{III}PPIX.

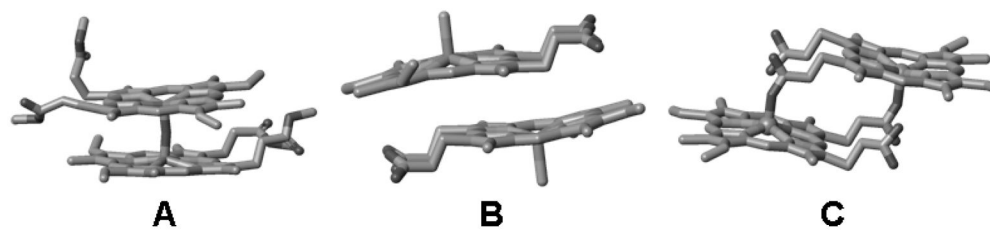


Figure 3. Structural Aspects of Hemozoin and its Analogues (such as β -Hematin, the Synthetic Equivalent of Hemozoin). (A) μ -oxo (μ -oxo bridged dimer of iron(III) protoporphyrin IX). (B) π - π dimer (π stacked iron(III) protoporphyrin IX dimer - for instance hemin dimer $[\text{Fe}^{\text{III}}\text{PPIX}(\text{Cl})_2]_2$). (C) μ -Pr (dimer formed by symmetrical and mutual intermolecular iron(III)-propionate coordination bonds in the particular case of $\text{Fe}^{\text{III}}\text{PPIX}$).

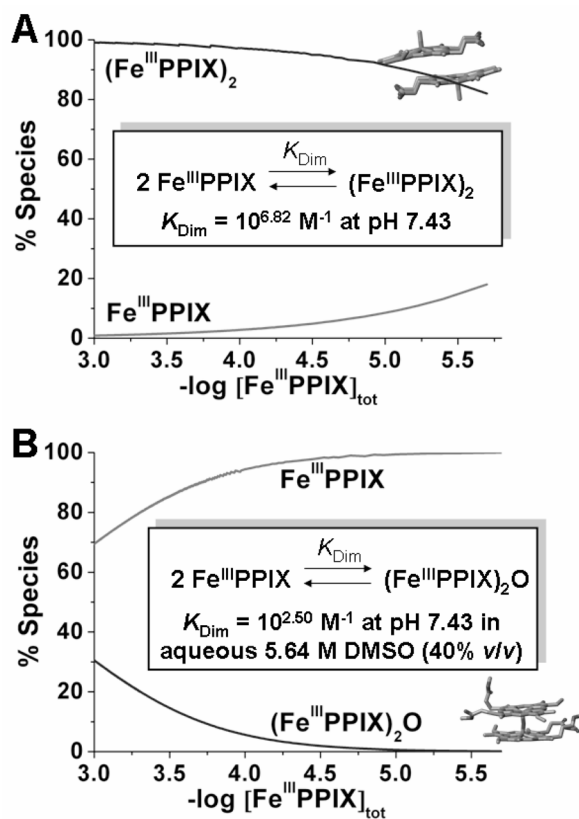


Figure 4. Speciation Diagrams of the Ferritroporphyrin IX (**Fe^{III}PPIX**) Species as a Function of $[\text{Fe}^{\text{III}}\text{PPIX}]_{\text{tot}}$ at 25 °C and pH 7.4. (A) Pure water; (B) aqueous 5.64 M DMSO (40 % v/v). Charges, solvent molecules, protons and hydroxides have been omitted in the equilibria given in the insets.

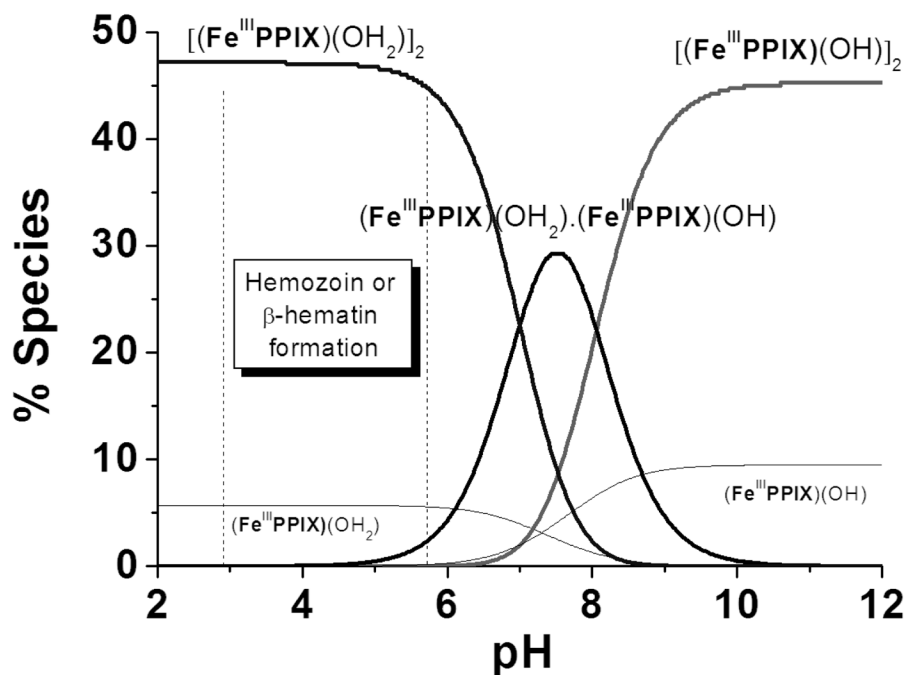


Figure 5. Thermodynamics of Ferriprotoporphyrin IX under Monomeric and π - π Dimeric States. Distribution Diagrams as a Function of pH of $\text{Fe}^{\text{III}}\text{PPIX}$ Species Calculated for $[\text{Fe}^{\text{III}}\text{PPIX}]_{\text{tot}} = 40 \mu\text{M}$. Thermodynamic data taken from reference [18] and [39]. H_2O and OH correspond to the $\text{Fe}(\text{III})$ axially coordinated molecules. Charges have been omitted for the sake of clarity.

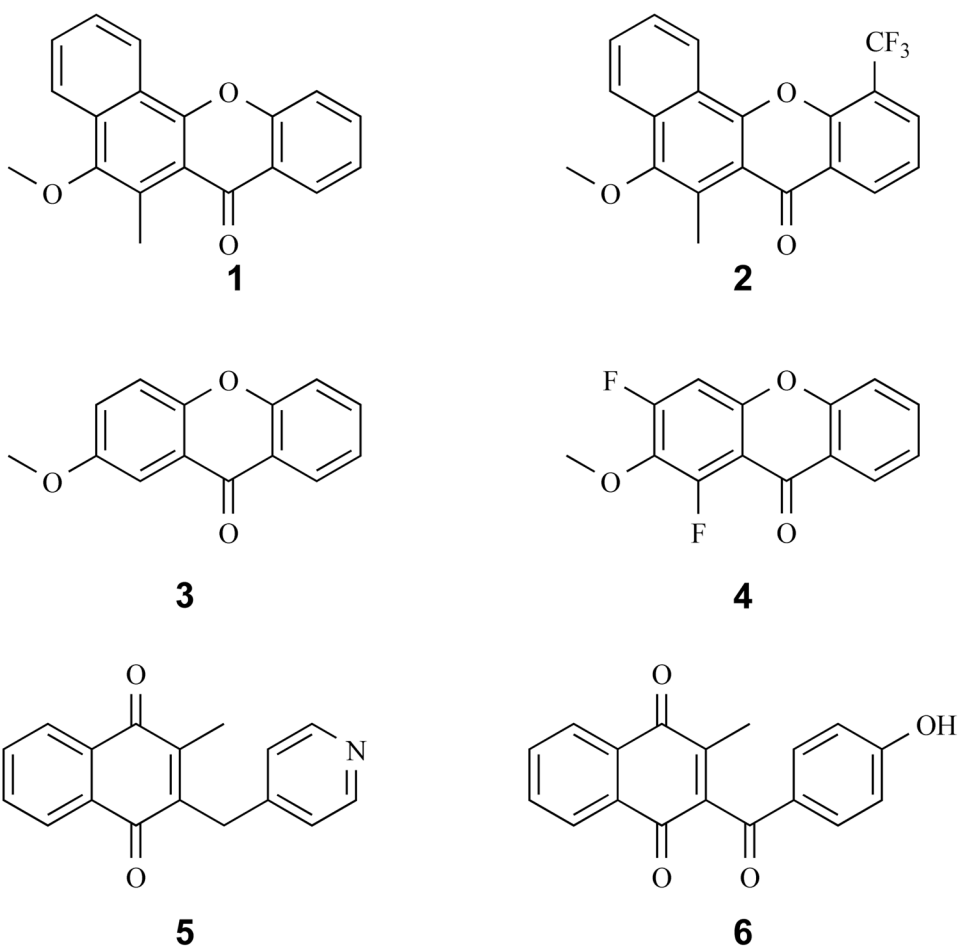


Figure 6. Chemical Structures of the Xanthenes and 1,4-Naphthoquinones Considered in this Work.

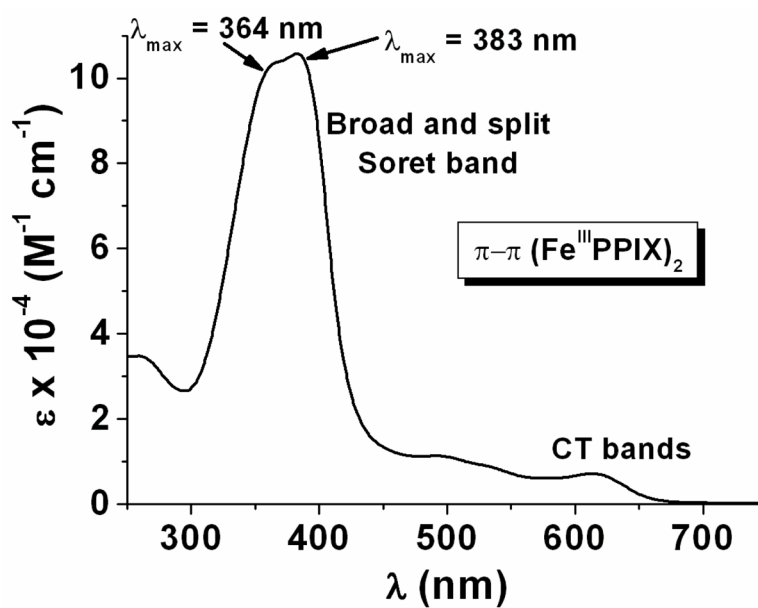
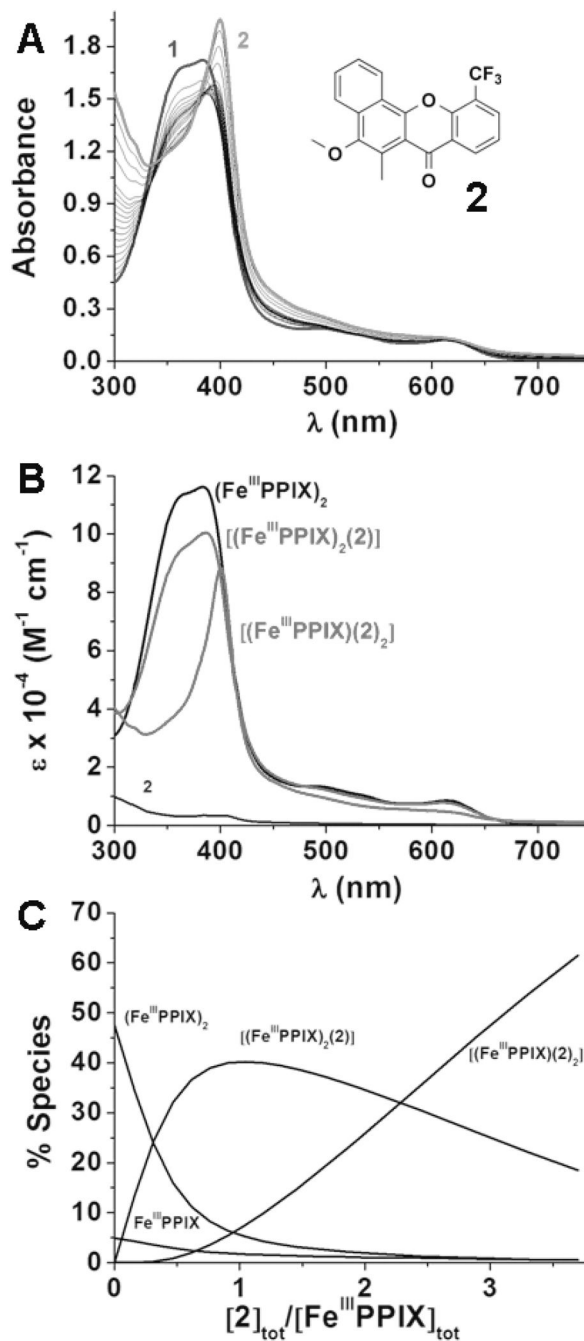


Figure 7. UV-visible Electronic Spectrum of Free Hematin under π - π Dimeric State Measured in 0.2 M Sodium HEPES Buffer pH 7.5 and at $T = 25 \text{ }^\circ\text{C}$.

**Figure 8.**

(A) Absorption Spectrophotometric Titration of Hematin (under a π - π Dimeric State) by Benzoxanthone **2**.

Solvent: 0.2 M sodium hepes buffer pH 7.5; $l = 1$ cm; $[\text{Fe}^{\text{III}}\text{PPIX}]_{\text{tot}} = 3.07 \times 10^{-5}$ M; (1) $[\text{2}]_{\text{tot}}/[\text{Fe}^{\text{III}}\text{PPIX}]_{\text{tot}} = 0$; (2) $[\text{2}]_{\text{tot}}/[\text{Fe}^{\text{III}}\text{PPIX}]_{\text{tot}} = 3.7$. (B) Absorption electronic spectra of the complexes formed between $\text{Fe}^{\text{III}}\text{PPIX}$ and substrate **2**. (C) Distribution diagrams as a function of $[\text{2}]_{\text{tot}}$ of the $\text{Fe}^{\text{III}}\text{PPIX}$ complexes formed with substrate **2** calculated for $[\text{Fe}^{\text{III}}\text{PPIX}]_{\text{tot}} = 3.07 \times 10^{-5}$ M.

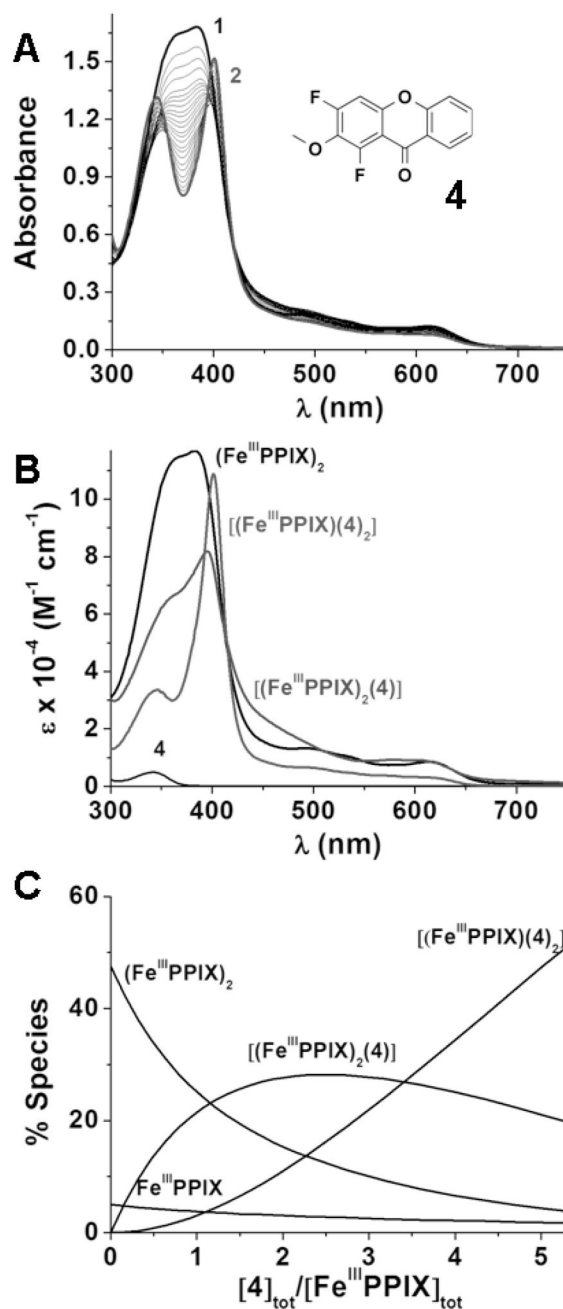


Figure 9.

(A) Absorption Spectrophotometric Titration of Hematin (under a π - π Dimeric State) by Xanthone **4**. Solvent: 0.2 M sodium hepes buffer pH 7.5; $l = 1$ cm; $[\text{Fe}^{\text{III}}\text{PPIX}]_{\text{tot}} = 3.0 \times 10^{-5}$ M; (1) $[\mathbf{4}]_{\text{tot}}/[\text{Fe}^{\text{III}}\text{PPIX}]_{\text{tot}} = 0$; (2) $[\mathbf{4}]_{\text{tot}}/[\text{Fe}^{\text{III}}\text{PPIX}]_{\text{tot}} = 5.33$. (B) Absorption electronic spectra of the complexes formed between $\text{Fe}^{\text{III}}\text{PPIX}$ and substrate **4**. (C) Distribution diagrams as a function of $[\mathbf{4}]_{\text{tot}}$ of the $\text{Fe}^{\text{III}}\text{PPIX}$ complexes formed with substrate **4** calculated for $[\text{Fe}^{\text{III}}\text{PPIX}]_{\text{tot}} = 3.0 \times 10^{-5}$ M.

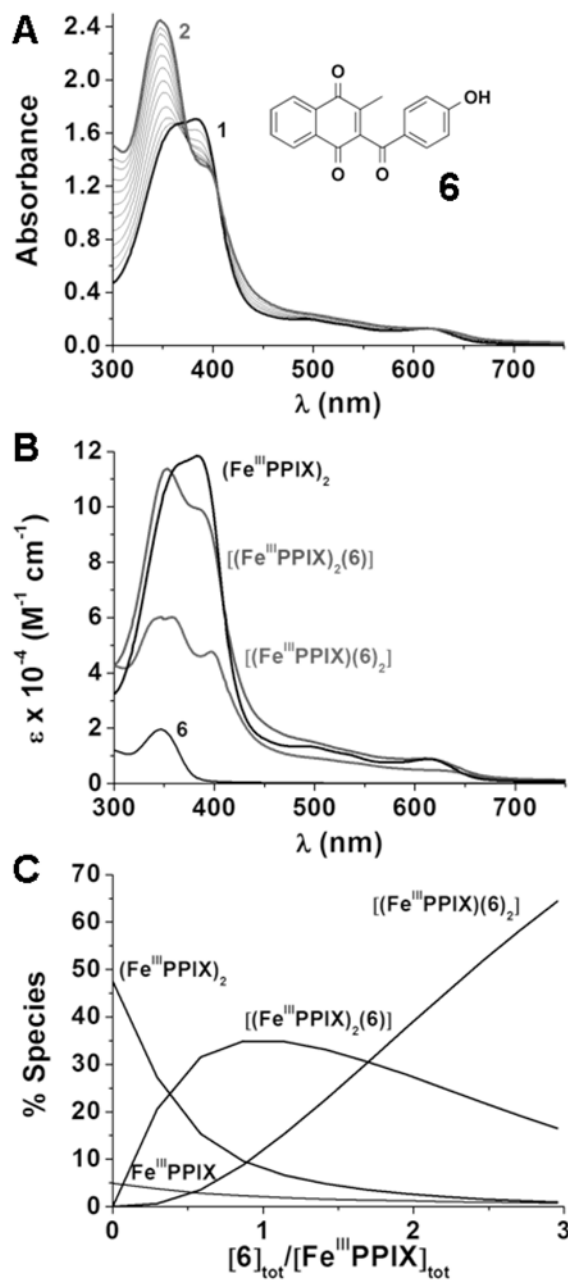


Figure 10.

(A) Absorption Spectrophotometric Titration of Hematin (in a π - π Dimeric State) by the Benzoylnaphthoquinone 6.

Solvent: 0.2 M sodium hepes buffer pH 7.5; $l = 1$ cm; $[\text{Fe}^{\text{III}}\text{PPIX}]_{\text{tot}} = 2.93 \times 10^{-5}$ M; (1)

$[\text{6}]_{\text{tot}}/[\text{Fe}^{\text{III}}\text{PPIX}]_{\text{tot}} = 0$; (2) $[\text{6}]_{\text{tot}}/[\text{Fe}^{\text{III}}\text{PPIX}]_{\text{tot}} = 2.96$. (B) Absorption electronic spectra

of the complexes formed between Fe^{III}PPIX and substrate 6. (C) Distribution diagrams as a

function of $[\text{6}]_{\text{tot}}$ of the Fe^{III}PPIX complexes formed with substrate 6 calculated at

$[\text{Fe}^{\text{III}}\text{PPIX}]_{\text{tot}} = 2.93 \times 10^{-5}$ M.

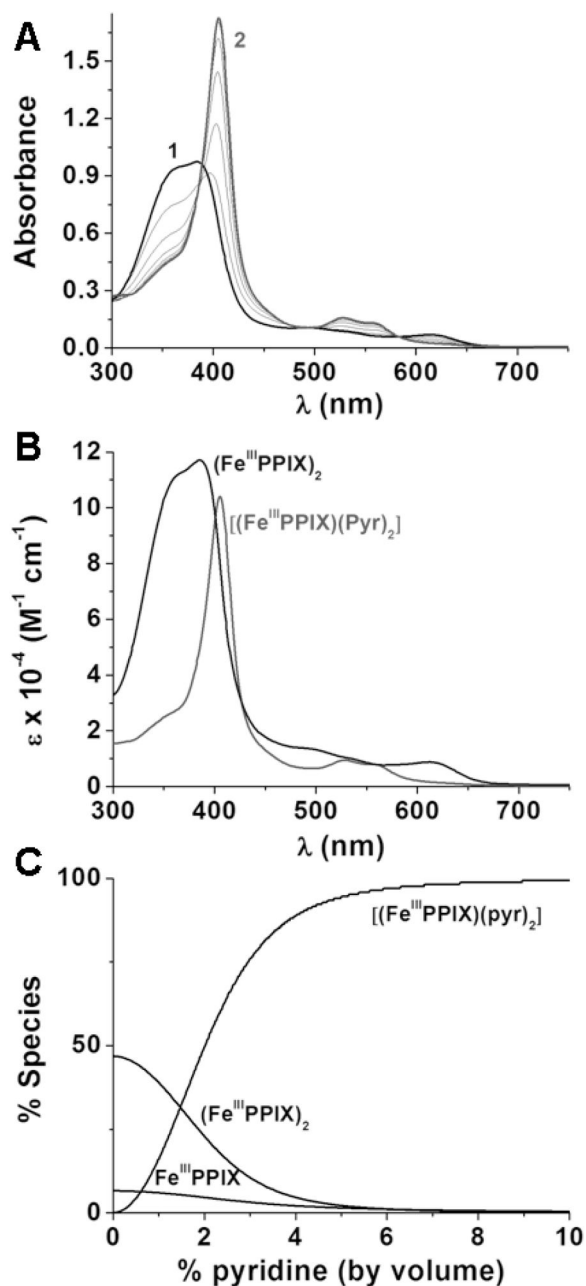


Figure 11.

(A) Absorption Spectrophotometric Titration of Hematin (in a π - π Dimeric State) by Pyridine (noted **Pyr**).

Solvent: 0.2 M sodium hepes buffer pH 7.5; $l = 1$ cm; $[\text{Fe}^{\text{III}}\text{PPIX}]_{\text{tot}} = 1.68 \times 10^{-5}$ M; (1) $[\text{Pyr}]_{\text{tot}}/[\text{Fe}^{\text{III}}\text{PPIX}]_{\text{tot}} = 0$; (2) $[\text{Pyr}]_{\text{tot}}/[\text{Fe}^{\text{III}}\text{PPIX}]_{\text{tot}} = 51667$. (B) Absorption electronic spectra of the complexes formed between $\text{Fe}^{\text{III}}\text{PPIX}$ and pyridine. (C) Distribution diagrams as a function of $[\text{Pyr}]_{\text{tot}}$ of the $\text{Fe}^{\text{III}}\text{PPIX}$ complexes formed with pyridine calculated at $[\text{Fe}^{\text{III}}\text{PPIX}]_{\text{tot}} = 1.68 \times 10^{-5}$ M. $\log \beta_{\text{Fe}^{\text{III}}\text{PPIX}(\text{Pyr})_2} = 2.25 \pm 0.05$ calculated in this study.

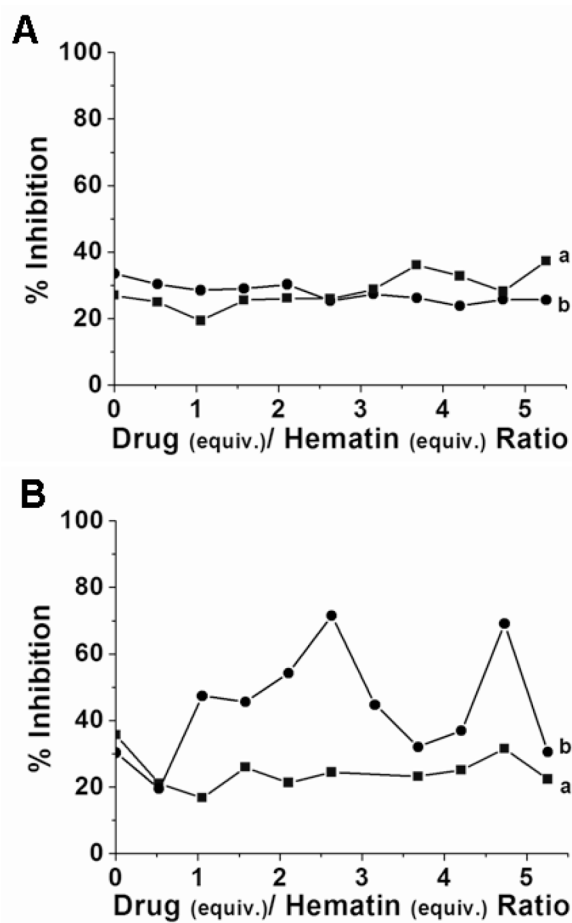


Figure 12.

Inhibition of β -Hematin Crystallization by (A) Benzoxanthone **1** and (B) Xanthone **3** Measured by UV-Visible Absorption Spectrophotometry using Pyridine (5% by volume) as Reporting Reagent. The squares (■) indicate the inhibition curve (a) obtained by addition of the drug prior to formation of β -hematin while the circles (●) represent the inhibition curve (b) obtained by addition of the drug after formation of β -hematin (hematin incubated at 60°C with 12.7 M acetate buffer at pH 4.5).

Solvent: 0.2 M + 0.02 M sodium hepes buffer pH 7.5, $T = 25$ °C.

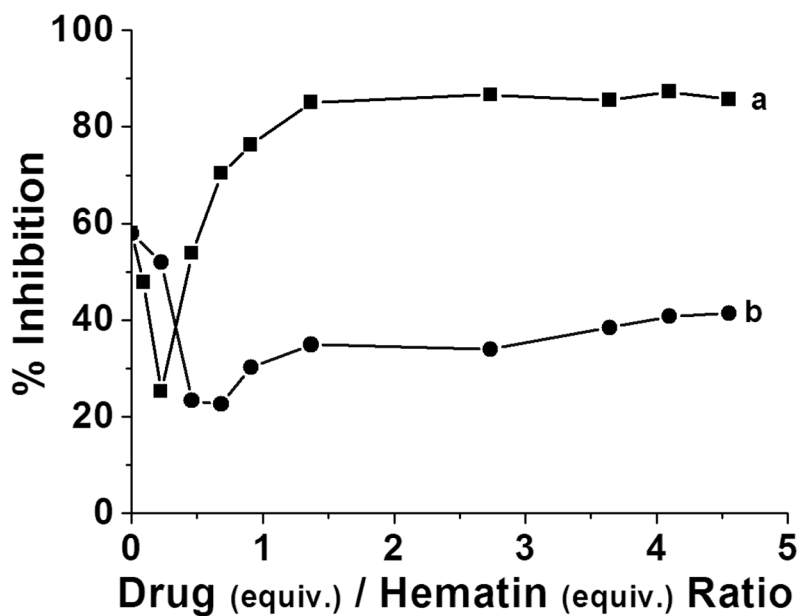


Figure 13. Inhibition of β -Hematin Crystallization by Amodiaquine Measured by UV-Visible Absorption Spectrophotometry using Pyridine (5% by volume) as Reporting Reagent. The squares (■) indicate the inhibition curve (a) obtained by addition of amodiaquine prior to formation of β -hematin while the circles (●) represent the inhibition curve (b) obtained by addition of amodiaquine after formation of β -hematin (hematin incubated at 60°C with 12.7 M acetate buffer at pH 4.5). Solvent: 0.2 M + 0.02 M sodium hepes buffer pH 7.5, $T = 25$ °C.

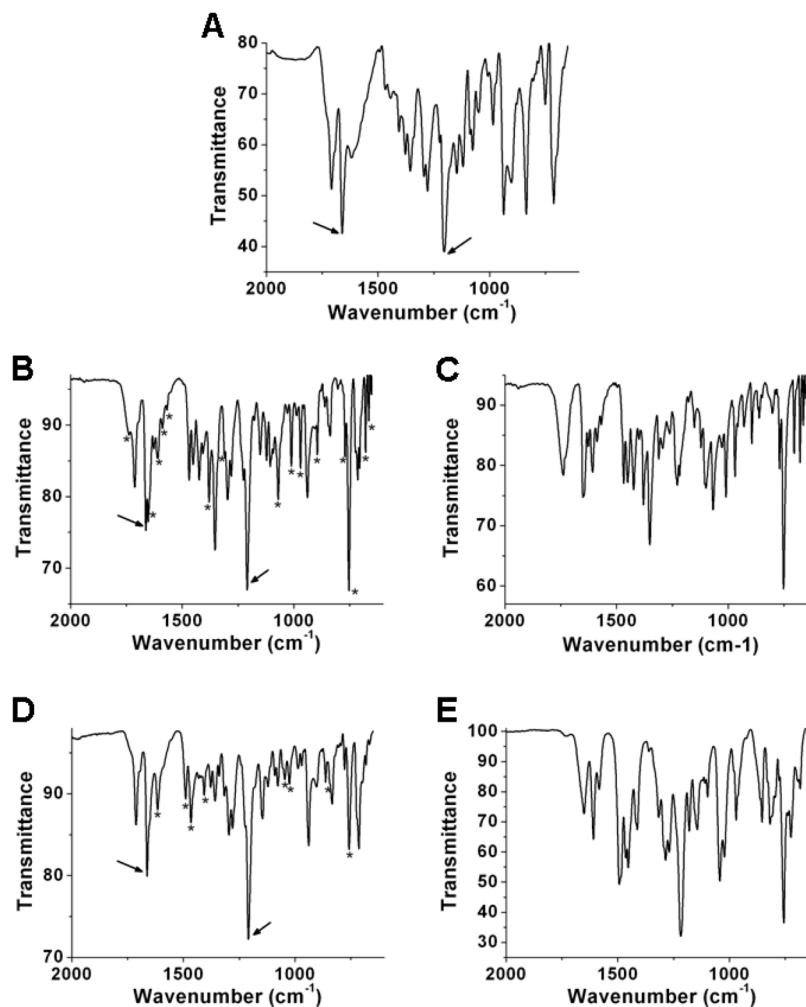


Figure 14.

Infrared Spectra of β -Hematin (**A**) and of Hematin Reaction Products with 3 Equivalents of Benzoxanthone **1** (**B**) and Xanthone **3** (**D**). (**A**) β -hematin prepared according to refs. [58] and [76] (1709(s), 1661(s), 1620(sh), 1467(w), 1444(w), 1406(s), 1377(s), 1356(s), 1338(sh), 1294(s), 1279(s), 1224(w), 1204(s), 1147(m), 1120(m), 1088(w), 1076(m), 1049(w), 1008(w), 985 (m), 937(s), 902(s), 836(s), 751(m), 712(s)). The peaks for β -hematin at 1661 cm^{-1} and 1204 cm^{-1} are indicated with arrows. Peaks due to the drug are marked with stars (*). IR spectra of benzoxanthone **1** (**C**) and xanthone **3** (**E**) are given for comparison purposes.

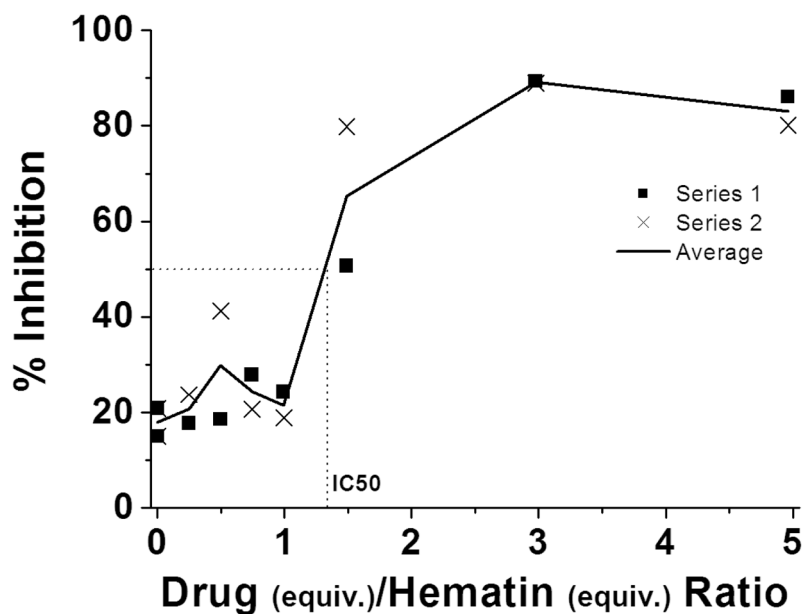


Figure 15. Inhibition of β -Hematin Crystallization by the Benzoyl-1,4-naphthoquinone **6** Measured by UV-Visible Absorption Spectrophotometry using Pyridine (5% by volume) as Reporting Reagent. Solvent: 0.2 M + 0.02 M sodium hepes buffer pH 7.5. The cross (×) and the square (■) labels correspond to two independent replicates, while the solid line corresponds to the averaged values.

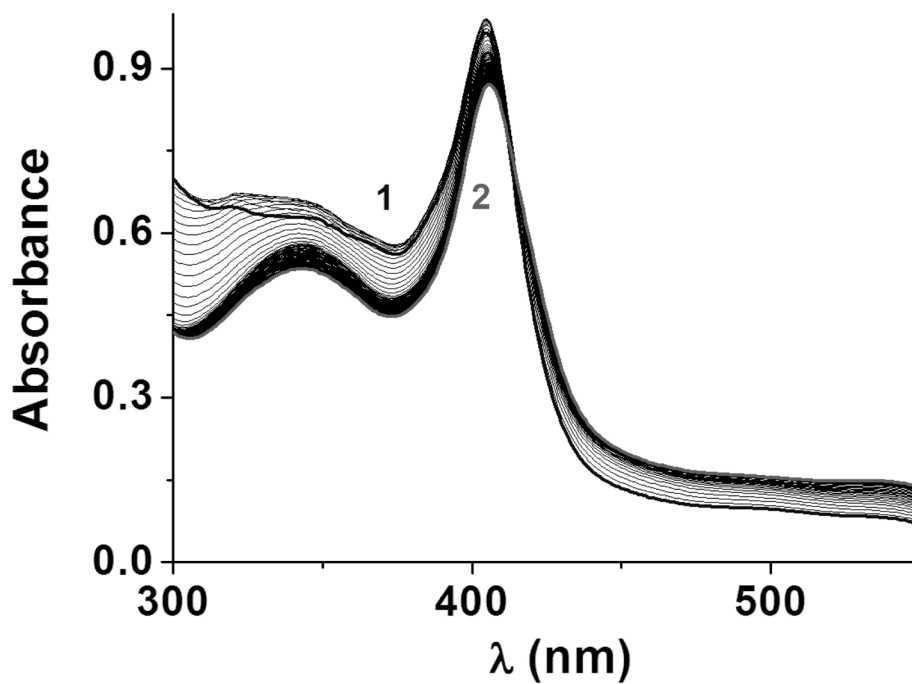


Figure 16. UV-Visible Absorption Spectra Recorded as a Function of Time and Showing the Absence of metHb(Fe^{III}) Reduction in the Coupled Assay with hGR/NADPH System in the Presence of Benzoxanthone 2.
Solvent: water (hGR acetate buffer pH 6.9 + 47 mM K₂PO₄ + 200 mM KCl); *T* = 37.0 °C; 40 μM NADPH + 66.5 nM hGR + 2 μM metHb + 40 μM benzoxanthone 2; (1) *t* = 0; (2) *t* ~ 60 min.

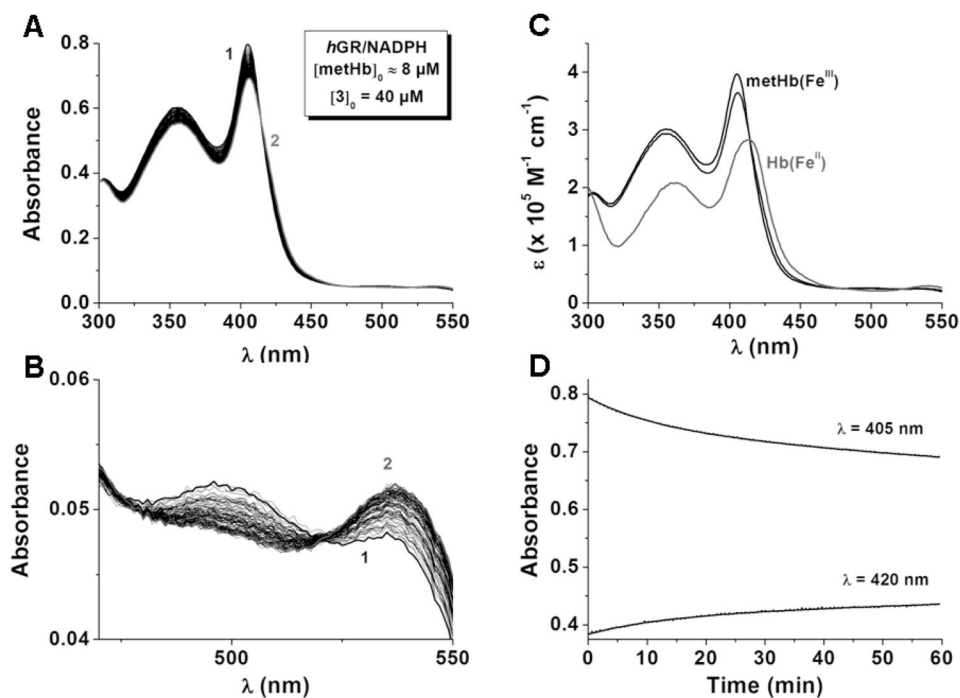


Figure 17. (A and B) UV-Visible Absorption Spectra Recorded as a Function of Time Showing the Slow metHb(Fe^{III}) Reduction in the Coupled Assay with the *hGR*/NADPH System in the Presence of Xanthone **3**. (C) Electronic Spectra of the Reactants and the Products of the metHb(Fe^{III}) Reduction. (D) Absorbance Changes at $\lambda = 405$ nm and $\lambda = 420$ nm. Solvent: water (*hGR* acetate buffer pH 6.9 + 47 mM K₂PO₄ + 200 mM KCl); $T = 37.0$ °C; 40 μ M NADPH + 133 nM *hGR* + 7.95 μ M metHb + 40 μ M **3**; (1) $t = 0$; (2) $t = 60$ min.

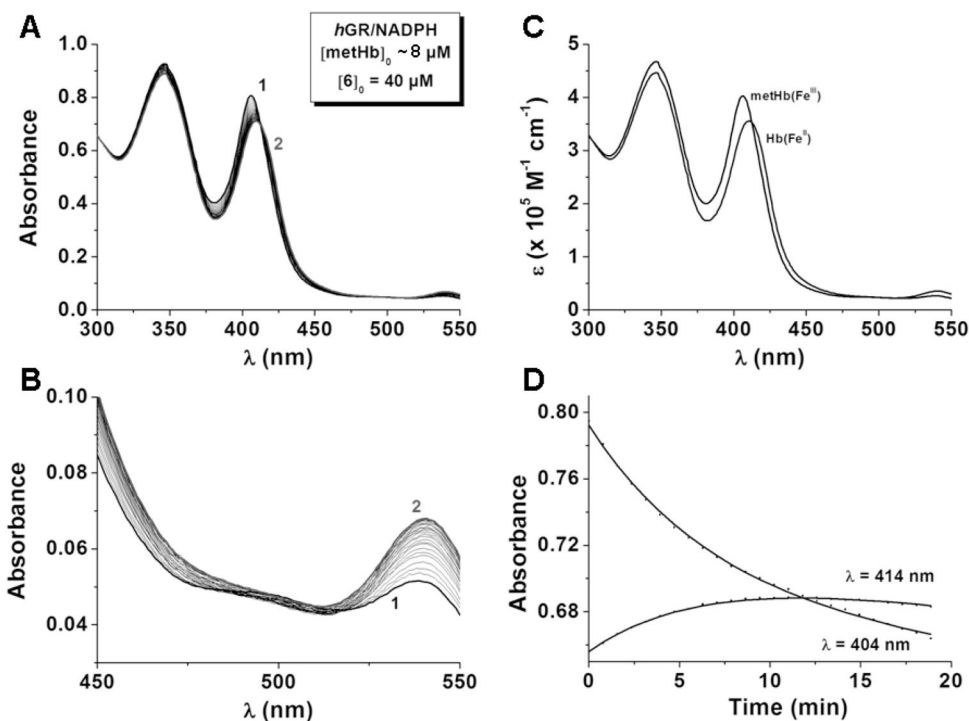


Figure 18. (A and B) UV-visible Absorption Spectra Recorded as a Function of Time Showing the fast $\text{metHb(Fe}^{\text{III}})$ Reduction in the Coupled Assay with the $hGR/NADPH$ System in the Presence of Benzoylnaphthoquinone **6**. (C) Electronic Spectra of the Reactants and the Products of the $\text{metHb(Fe}^{\text{III}})$ Reduction. (D) Absorbance Changes at $\lambda = 404 \text{ nm}$ and $\lambda = 414 \text{ nm}$. Solvent: water (hGR acetate buffer pH 6.9 + 47 mM K_2PO_4 + 200 mM KCl); $T = 37.0 \text{ }^\circ\text{C}$; 40 μM NADPH + 133 nM hGR + 7.95 μM metHb + 40 μM **3**; (1) $t = 0$; (2) $t \sim 19 \text{ min}$.

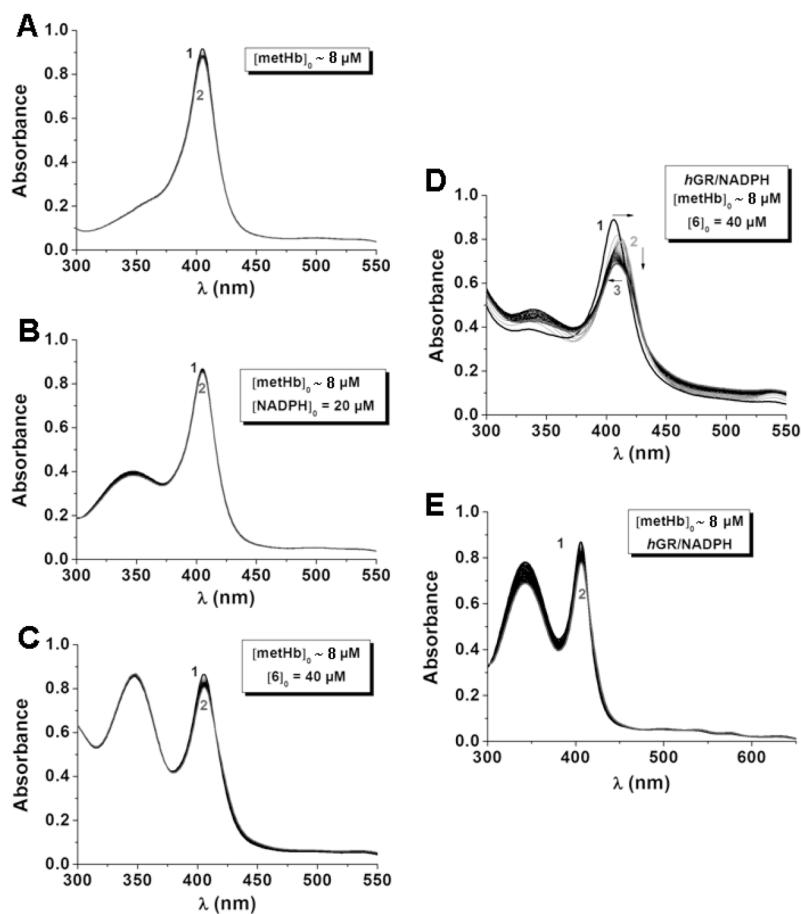
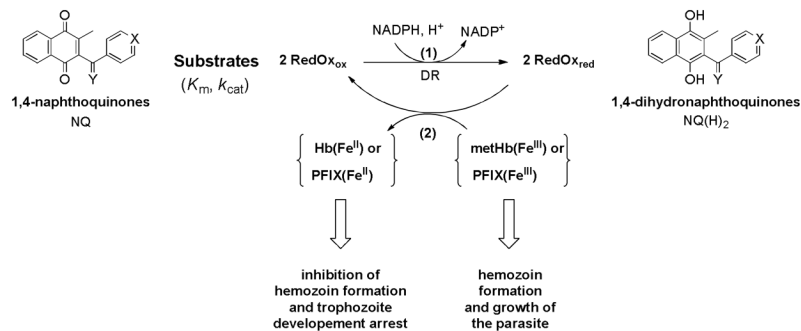


Figure 19.

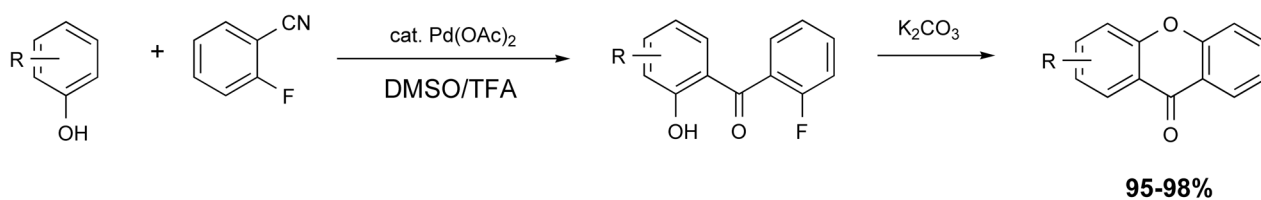
UV-Visible Absorption Spectra Recorded as a Function of Time Showing the Influence of the Reduced Substrates on the methHb(Fe^{III}) Reduction in the Coupled Assay with the *hGR*/NADPH System.

Solvent: water (*hGR* acetate buffer pH 6.9 + 47 mM K_2PO_4 + 200 mM KCl) (A) 7.95 μM methHb. (B) 7.95 μM methHb + 40 μM NADPH. (C) 7.95 μM methHb + 40 μM **3**. (D) 40 μM NADPH + 133 nM *hGR* + 7.95 μM methHb + 40 μM **3**. For A, B, C and D: (1) $t = 0$; (2) $t = 60$ min. (E) 100 μM NADPH + 133 nM *hGR* + 7.95 μM methHb, (1) $t = 0$; (2) $t = 120$ min.

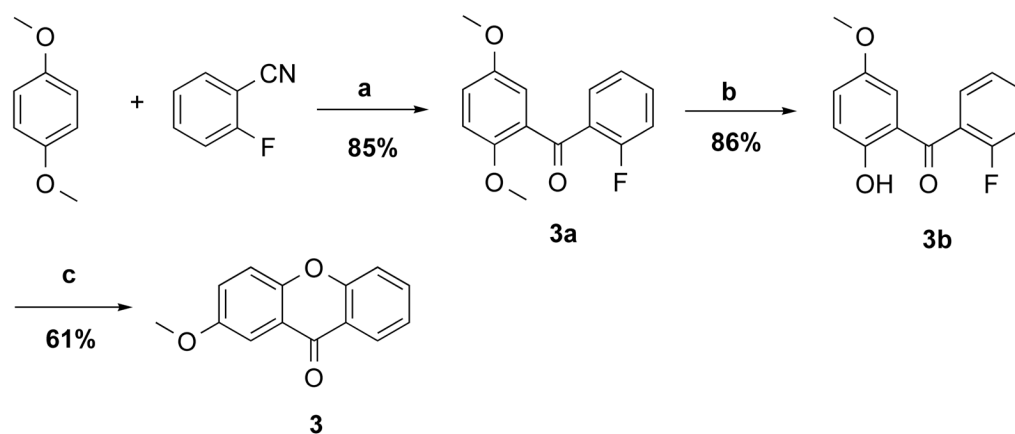
**Scheme 1.**

Redox-Active Compounds as Subversive Substrates of NADPH-Dependent Disulfide Reductases.^{a,b} RedOx stands for the redox-active agents like methylene blue, 1,4-naphthoquinones (given as an example in this scheme) or xanthenes. The labels ox and red stand for the oxidized and reduced states of these redox active agents, respectively.

^a DR means disulfide reductase; ^b X is the series variable, Y means H₂ or O.



Scheme 2.
A Palladium-Catalyzed Two-Step Strategy to Access Xanthenes.

**Scheme 3.**Synthesis of 2-Methoxy-9H-xanthen-9-one **3**.Reagents and conditions: a) 0.1 equiv. Pd(OAc)₂, DMSO/TFA, 95°C, 24h; b) 1.0 equiv. BBr₃, DCM, 0°C, 1h; c) 2.0 equiv. K₂CO₃, acetone, 50°C, 2h.

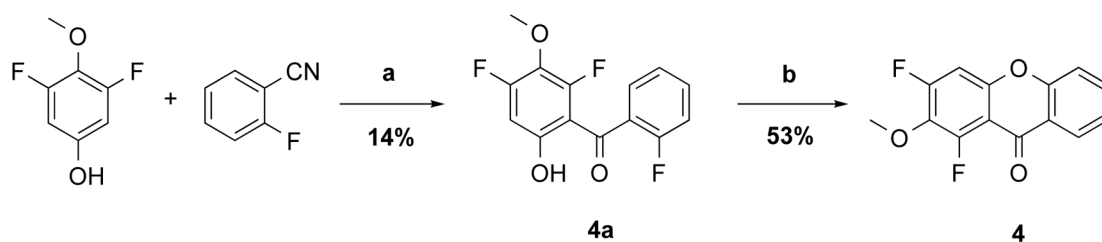
**Scheme 4.**Synthesis of 2,4-Difluoro-3-methoxy-9H-xanthen-9-one **4**.Reagents and conditions: a) 0.1 equiv. Pd(OAc)₂, DMSO/TFA, 95°C, 24h; b) 2.0 equiv.K₂CO₃, acetone, 50°C, 2h.

Table 1

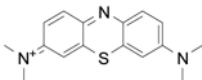
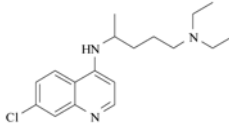
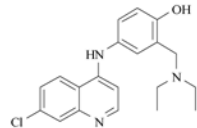
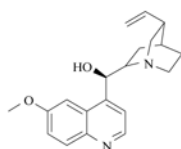
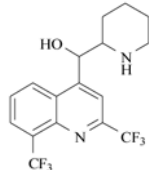
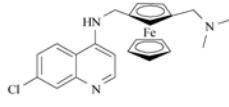
Definition and Abbreviation of the Heme-Containing Compounds Cited in this Work.^a

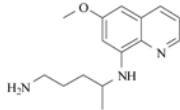
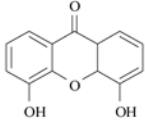
Heme compound	Abbreviation	Definition
Heme	Heme Fe^{II}PPIX	Prosthetic group that consists of an iron atom contained in the center of a heterocyclic porphyrin ring, namely the protoporphyrin IX (see Figure 2). It corresponds to the active protein-free unit of hemoglobin molecule.
Hemoglobin	Hb(Fe ^{II}) or Hb	Oxygen-carrying Fe(II) hemoprotein of erythrocytes made up of four different polypeptide globin chains that contain between 141 and 146 amino acids and a Fe^{II}PPIX active site.
Oxyhemoglobin	oxyHb(Fe ^{II}) or oxyHb	Hemoglobin protein containing an oxygen molecule in its Fe^{II}PPIX site
Methemoglobin	metHb(Fe ^{III}) or metHb	Hematogenous pigment formed from hemoglobin by oxidation of the iron atom from the ferrous to the ferric state. A small amount is found in the blood normally, but injury or toxic agents convert a larger proportion of hemoglobin into methemoglobin, which does not function as an oxygen carrier.
Hemin chloride	Hemin Fe^{III}PPIXCl	Heme containing a chloride anion axially bound in the fifth position of the iron(III) porphyrinic system.
Hematin	Hematin Fe^{III}PPIX(OH₂) or Fe^{III}PPIX(OH)	Heme containing a water or a hydroxide molecule axially bound in the fifth position of the iron(III) porphyrinic system.
μ -Oxo hematin dimer	μ -oxo Fe^{III}PPIX dimer	μ -oxo bridged dimer of iron(III) protoporphyrin IX
π - π Hematin dimer	π - π Fe^{III}PPIX dimer	π stacked iron(III) protoporphyrin IX dimer
μ -Pr hematin dimer	μ -Pr Fe^{III}PPIX dimer	Dimer formed by symmetrical and mutual intermolecular iron(III)-propionate coordination bonds in the particular case of Fe^{III}PPIX
β -hematin	β -hematin	Synthetic hematin crystal standing for hemozoin pigment equivalent
Hemozoin or malarial pigment	Hz	Disposal pigment – biocrystals which result from self-association of Fe(III) protoporphyrin IX - formed during the digestion of methemoglobin in several blood-feeding parasites (the Fe^{III}PPIX are held together mainly through π - π and μ -Pr interactions).

^aRefer to references [20], [35] [39], [40] and [41] for schematic representation of μ -oxo **Fe^{III}PPIX**, π - π **Fe^{III}PPIX** and μ -Pr **Fe^{III}PPIX** dimers and X-ray structures of β -hematin and hemozoin.

Table 2

Apparent Association Constants of Quinoline and Xanthone Based Drugs with Hematin or Hemin in Aqueous Solution.^a

Compound	Apparent association constant log K_A		
	Aqueous 5.64 M DMSO/ Drug:Heme	Water/ Drug:Heme	Water [57]/ Drug:Heme
 Methylene blue		5.5 ^b 1:2 [25]	
 Chloroquine	5.52 ± 0.03 ^b 1:1 [58]	5.6 ^c 1:4 [60]	3.02 ^{d,f} 1:1 5.11 ^{b,f} 1:1
 Amodiaquine	5.39 ± 0.04 ^b 1:1 [58]	4.97 ^c 1:4 [60]	3.26 ^{d,f} 1:1 6.38 ^{d,f} 2:1
 Quinine	4.10 ± 0.02 ^b 1:1 [58]	4.32 ^c 1:5 [60]	3.0 ^{d,f} 1:1 5.10 ^{d,f} 2:1
 Mefloquine	3.90 ± 0.08 ^b 1:1 [58]	4.08 ^c 1:3 [60]	3.70 ^{d,f} 1:1 4.43 ^{d,f} 2:1
 Ferroquine	4.95 ± 0.05 ^b 1:1 [61]		
Ferroquine	5.52 ± 0.03 ^b 1:1 [62]		

Compound	Apparent association constant $\log K_A$		
	Aqueous 5.64 M DMSO/ Drug:Heme	Water/ Drug:Heme	Water [57]/ Drug:Heme
 Primaquine	Not detectable [58]	4.2 ^c 1:7 [60]	
 4,5-dihydroxyxanthenones		5.29 ^e 1:2	

^aIn aqueous 5.64 M DMSO (40% v/v) at pH 7.43, the predominant species for $[\text{Fe}^{\text{III}}\text{PPIX}]_{\text{tot}} < 10^{-2.5}$ M is most likely the (OH/H₂O)-monomer (Figure 4b), while the heme π - π dimer predominates in water (Figure 4a).

^bpH 7.43–7.5.

^cpH 6.5.

^dpH 5.6.

^epH 5.8.

^fInteractions with hemin chloride. $T = 22.5$ – 28.5 °C.

Table 3

Summary of the Binding Studies Between the Substrates Considered in this Work and Hematin π - π Dimer at pH 7.5 and $T=25^\circ\text{C}$ (sh = shoulder).

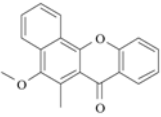
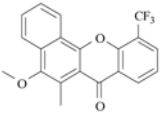
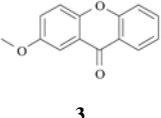
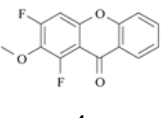
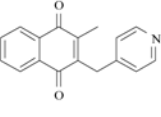
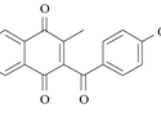
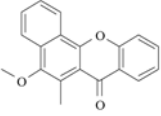
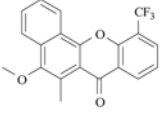
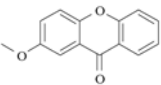
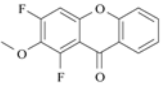
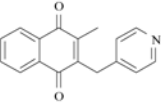
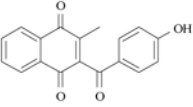
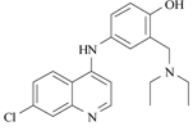
Substrate	Association constant Heme:drug	Dissociation constant K_D (μM)	λ_{max} (e^{max}) nm ($\times 10^4 \text{ M}^{-1} \text{ cm}^{-1}$)
 1	1:1 $\log K_{11} = 5.9 \pm 0.1$	1.26	400 (5.18) sh 355 (2.9)
 2	2:1 $\log \beta_{21} = 12.5 \pm 0.1$ 1:2 $\log \beta_{12} = 10.2 \pm 0.2$	2.00	386 (10.0) sh 359 (9.3) 401 (8.82)
 3	1:1 $\log K_{11} = 5.78 \pm 0.03$	1.66	399 (4.4) sh 357 (3.41)
 4	2:1 $\log \beta_{21} = 11.4 \pm 0.1$ 1:2 $\log \beta_{12} = 9.2 \pm 0.2$	25.1	395 (8.18) sh 357 (6.51) 401 (10.9) sh 357 (3.37)
 5	2:1 $\log \beta_{21} = 12.6 \pm 0.2$ 1:2 $\log \beta_{12} = 10.6 \pm 0.2$	1.58	386 (9.76) sh 361 (9.3) 400 (5.55) sh 342 (3.08)
 6	2:1 $\log \beta_{21} = 12.4 \pm 0.3$ 1:2 $\log \beta_{12} = 10.6 \pm 0.3$	2.63	386 (9.90) 353 (11.38) 397 (4.76) 353 (6.02)

Table 4

Summary of the Hematin Crystallization Inhibition Assay with the Xanthone, Benzoxanthone and 1,4-Naphthoquinone Derivatives. (ni = no inhibition)

Substrate	IC ₅₀ (equivalent inhibitor)	%max Inhibition
 1	ni	~ 28% at 5 equiv. ^a ~ 28% at 5 equiv. ^b
 2	ni	~ 23% at 5 equiv.
 3	ni	~ 25% at 5 equiv. ^a ~ 44% at 5 equiv. ^b
 4	ni	~ 26% at 5 equiv.
 5	4.3 equiv.	~ 80%
 6	1.3 equiv.	~ 90%
 Amodiaquine	0.4 equiv.	~ 86% at 5 equiv. ^a ~ 40% at 5 equiv. ^b

^aWith no β -hematin preformed.

^bWith β -hematin preformed (hematin incubated at 60°C for 60 mins with 12.7 M acetate buffer at pH 4.5)

Table 5

Summary of the Kinetic Studies of metHb(Fe^{III}) Reduction by Xanthone, Benzoxanthone and Naphthoquinone Substrates.

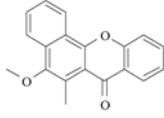
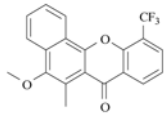
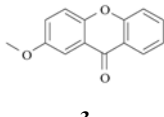
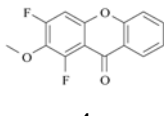
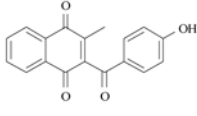
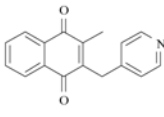
Substrate	Kinetic parameters k_{obs} (s ⁻¹)/ $t^{red}_{1/2}$ (min)	Spectroscopic characteristics $\epsilon^{\lambda_{max}}$ (M ⁻¹ cm ⁻¹)
 1	No metHb(Fe ^{III}) → oxyHb(Fe ^{II}) reaction	
 2	No metHb(Fe ^{III}) → oxyHb(Fe ^{II}) reaction	
 3	$(7 \pm 2) \times 10^{-5} \text{ s}^{-1}$ 165 min	metHb: $\epsilon^{405} = 9.97 \times 10^4 \text{ M}^{-1} \text{ cm}^{-1}$ oxyHb: $\epsilon^{412} = 7.11 \times 10^4 \text{ M}^{-1} \text{ cm}^{-1}$ oxyHb: $\epsilon^{541} = 7.40 \times 10^3 \text{ M}^{-1} \text{ cm}^{-1}$
 4	$(1.2 \pm 0.2) \times 10^{-4} \text{ s}^{-1}$ 96.3 min	metHb: $\epsilon^{405} = 1.02 \times 10^5 \text{ M}^{-1} \text{ cm}^{-1}$ oxyHb: $\epsilon^{408} = 7.78 \times 10^4 \text{ M}^{-1} \text{ cm}^{-1}$ oxyHb: $\epsilon^{538} = 7.75 \times 10^3 \text{ M}^{-1} \text{ cm}^{-1}$
 6	$(2.5 \pm 0.1) \times 10^{-3} \text{ s}^{-1}$ 4.6 min	metHb: $\epsilon^{406} = 1.01 \times 10^5 \text{ M}^{-1} \text{ cm}^{-1}$ oxyHb: $\epsilon^{409} = 9.20 \times 10^4 \text{ M}^{-1} \text{ cm}^{-1}$ oxyHb: $\epsilon^{540} = 8.82 \times 10^3 \text{ M}^{-1} \text{ cm}^{-1}$
 5	$(1.95 \pm 0.02) \times 10^{-3} \text{ s}^{-1}$ 5.9 min	metHb: $\epsilon^{405} = 1.11 \times 10^5 \text{ M}^{-1} \text{ cm}^{-1}$ oxyHb: $\epsilon^{409} = 9.49 \times 10^4 \text{ M}^{-1} \text{ cm}^{-1}$ oxyHb: $\epsilon^{541} = 1.00 \times 10^4 \text{ M}^{-1} \text{ cm}^{-1}$

Table 6Experimental conditions used for the β -Hematin inhibition assay.

Drug (equiv.) /Hematin (equiv.) ratio	Concentration (mM)	Volume of stock solution (μ L)	Volume of DMSO	Final [drug] ₀ in the Eppendorf tube (mM)
5	89.1	15	0	4.96
3	53.5	9	6	2.98
1.5	26.7	4.5	10.5	1.45
1	17.8	3	12	0.99
0.75	13.4	2.25	12.75	0.75
0.5	8.9	1.5	13.5	0.5
0.25	4.5	0.75	14.25	0.25
0	0	0	15	0